

QUANTUM MECHANICAL CLOSURE OF PARTIAL DIFFERENTIAL EQUATIONS WITH SYMMETRIES*

CHRIS VALES[†], DAVID C. FREEMAN[†], JOANNA SLAWINSKA[†], AND DIMITRIOS GIANNAKIS[†]

Abstract. We develop a framework for the dynamical closure of spatiotemporal dynamics governed by partial differential equations. We employ the mathematical framework of quantum mechanics to embed the original classical dynamics into an infinite dimensional quantum mechanical system, using the space of quantum states to model the unresolved degrees of freedom of the original dynamics and the technology of quantum measurement to predict their contributions to the resolved dynamics. We use a positivity preserving discretization to project the embedded dynamics to finite dimension. Combining methods from operator valued kernels and delay embedding, we derive a compressed representation of the dynamics that is invariant under the spatial symmetries of the original dynamics. We develop a data driven formulation of the scheme that can be realized numerically and apply it to a dynamical closure problem for the shallow water equations, demonstrating that our closure model can accurately predict the main features of the true dynamics, including for out of sample initial conditions.

Key words. dynamical closure, parametrization, quantum mechanics, kernel methods, delay embedding, transfer operators, shallow water equations.

1. Introduction. Complex dynamical systems often encompass degrees of freedom that evolve over a wide range of temporal and spatial scales, with their evolution depending on different physical regimes. A challenging problem in such multiscale, multiphysics systems is trying to include dynamical information for degrees of freedom that either are too computationally expensive to simulate directly or depend on fully or partially unknown physical processes [14].

The approach employed by *closure* or *parametrization* methods is to derive surrogate dynamical models that can be used to approximate the contributions of fine grain degrees of freedom to the dynamics of coarse grain processes we can simulate consistently. Such approaches have their origin in climate dynamics and turbulence research [38, 33, 1, 18], but have since found consequential applications in a wide range of fields [15].

Mathematically, closure methods depend on a separation of the state space of the original dynamical system into two components: (1) the resolved degrees of freedom, which represent the coarse grain processes we can simulate or measure consistently and with tractable cost; (2) the unresolved degrees of freedom, which are considered too complex or expensive to simulate or measure directly. Once the unresolved degrees of freedom have been identified, one has to define a surrogate model for their *fluxes*—namely, their contributions—to the resolved dynamics. How to define such a model, and whether such a model should be deterministic or stochastic, are active areas of research that use various mathematical tools to offer alternative approaches to this problem [14, 29, 2].

One approach toward this problem is defining a surrogate model as a functional

* Corresponding author: Chris Vales (chris.vales@dartmouth.edu).

Funding: DG and JS acknowledge support from the U.S. Department of Energy under grant DE-SC0025101. CV was supported as a postdoctoral researcher from this grant. DG acknowledges support from the U.S. Department of Defense, Basic Research Office under Vannevar Bush Faculty Fellowship grant N00014-21-1-2946. DCF was supported as a PhD student from this grant.

[†]Department of Mathematics, Dartmouth College, Hanover, NH 03755, USA (chris.vales@dartmouth.edu, david.c.freeman.gr@dartmouth.edu, joanna.m.slawska@dartmouth.edu, dimitrios.giannakis@dartmouth.edu).

relationship between the resolved and unresolved degrees of freedom. In this way, the unresolved variables are determined by a deterministic function of the resolved variables. Early attempts to define such functions depended on expert knowledge of the underlying physical process being modeled, featuring formulas that try to predict the averaged fluxes to the resolved variables. More recently, an alternative data driven approach has emerged, where functional relationships are not derived based on expert physical reasoning but are discovered by analyzing large amounts of numerical or experimental data [5, 7, 8, 24, 28, 30, 32, 44].

Modeling the unresolved degrees of freedom by a deterministic function of the resolved degrees corresponds to a reduction in the dimension of the full state space of the original dynamics. Regardless of the complexity of the employed functional relationship, any dynamical independence the unresolved variables had has been relinquished. One important consequence of this reduction in state space dimension is that the resulting parametrized system may experience a loss in its ability to produce complex spatiotemporal behavior such as chaotic dynamics [27]. If that happens, the developed parametrized system will inevitably struggle to consistently approximate the original dynamics.

To address the issue of dimension reduction and the potential loss of complex dynamics, one approach has been to use stochastic methods to model the unresolved degrees of freedom, instead of deterministic ones [10, 2, 29]. In this way, the surrogate unresolved variables retain some of their dynamical independence from the resolved variables, and the state space of the parametrized system is not reduced to the resolved state space.

Independently of whether the unresolved variables are represented using a deterministic or stochastic framework, the main goal of closure methods is to construct a surrogate model that can accurately and consistently approximate the original dynamics. Additionally, it should do so with a tractable computational cost and without imposing a strong reduction in the complexity of the predicted dynamical behavior.

In the present work we extend the framework developed in [20, 16, 17] to the closure of spatiotemporal dynamics, modeling the unresolved dynamics using a quantum mechanical system. More specifically, the unresolved degrees of freedom are represented by quantum density operators and the fluxes by quantum observables, while the generation of the required flux terms is carried out using tools from the mathematical theory of quantum measurement [23, 34, 36]. The closure framework can be used to derive both deterministic and stochastic surrogate models; in this work we focus on the deterministic setting. In addition to structure preservation properties [16, 17], our proposed scheme can be realized numerically in a data driven fashion using kernel integral operator methods [3, 19] and spectral analysis of vector valued observables [22]. Relying on operator theoretic methods in Hilbert spaces, the data driven framework has the additional benefit of a rigorous consistency proof in the limit of infinite training data under reasonable assumptions [16, 17].

1.1. Problem statement. We consider a dynamical system $\Phi^t : X \rightarrow X$, $t \geq 0$, on an infinite dimensional state space X possessing an ergodic invariant probability measure μ with compact support. The flow map Φ^t represents the spatiotemporal dynamics governed by a partial differential equation on a spatial domain S . As such, elements of state space X are functions on the spatial domain S ; more specifically, we consider $X \subset L^2(S, \nu; \mathbb{R})$ with ν denoting the Lebesgue measure on S .

We assume that there exists a symmetry group G' acting on the spatial domain S with a continuous left action $\Gamma_{S,g} : S \rightarrow S$, $g \in G'$ which preserves the null sets

of measure ν . The action $\Gamma_{S,g}$ induces the action on state space $\Gamma_{X,g} : X \rightarrow X$, $\Gamma_{X,g}(x) = x \circ \Gamma_{S,g}^{-1}$, $g \in G'$. The actions of group G' on X represent dynamical symmetries of the dynamics Φ^t ; namely, we assume the following equivariance property

$$\Gamma_{X,g} \circ \Phi^t = \Phi^t \circ \Gamma_{X,g}$$

for all $t \geq 0$, $g \in G'$.

We decompose the state space $X = \mathcal{X} \times \mathcal{Y}$ with \mathcal{X} denoting the state space of the resolved degrees of freedom of the dynamics and \mathcal{Y} the state space of the unresolved degrees. In the present work we operate under the assumption that the resolved state space \mathcal{X} is a finite dimensional differentiable manifold that can be embedded into $\mathbb{R}^{d'}$ for some $d' \in \mathbb{N}$. In many applications it is natural to assume that \mathcal{X} is finite dimensional. For instance many dissipative partial differential equations give rise to long time dynamics that is confined to a finite dimensional subset of their state space [37]. In other cases discretization of the differential operator modeling the considered dynamics also yields a finite dimensional state space.

We introduce a flux space $\mathcal{Z} = \mathbb{R}^d$, $d \in \mathbb{N}$, and flux map $Z : \mathcal{Y} \rightarrow \mathcal{Z}$ which will allow us to include in the resolved dynamics terms that depend on the unresolved variables. Based on our decomposition of state space X we define the flow maps for the resolved dynamics $\Phi_{\mathcal{X}}^t : \mathcal{X} \times \mathcal{Z} \rightarrow \mathcal{X}$, $\Phi_{\mathcal{X}}^t = \text{proj}_{\mathcal{X}} \circ \Phi^t$ and unresolved dynamics $\Phi_{\mathcal{Y}}^t : \mathcal{X} \times \mathcal{Y} \rightarrow \mathcal{Y}$, $\Phi_{\mathcal{Y}}^t = \text{proj}_{\mathcal{Y}} \circ \Phi^t$, where proj_A denotes the canonical projection onto a subspace A . With these definitions in place, the dynamics Φ^t can be expressed as

$$\Phi^t(\hat{x}, y) = (\Phi_{\mathcal{X}}^t(\hat{x}, Z(y)), \Phi_{\mathcal{Y}}^t(\hat{x}, y))$$

with state vector $(\hat{x}, y) \in \mathcal{X} \times \mathcal{Y}$.

Our goal in this work is to construct surrogate dynamics $\tilde{\Phi}^t : \tilde{X} \rightarrow \tilde{X}$ in a surrogate state space $\tilde{X} = \mathcal{X} \times \tilde{\mathcal{Y}}$ where $\tilde{\mathcal{Y}}$ denotes a surrogate unresolved state space. Based on our distinction between \mathcal{Y} and $\tilde{\mathcal{Y}}$ we also introduce a surrogate version of the flux map $\tilde{Z} : \tilde{\mathcal{Y}} \rightarrow \mathcal{Z}$. The surrogate dynamics $\tilde{\Phi}^t$ can now be expressed as

$$\tilde{\Phi}^t(\hat{x}, \tilde{y}) = (\tilde{\Phi}_{\mathcal{X}}^t(\hat{x}, \tilde{Z}(\tilde{y})), \tilde{\Phi}_{\tilde{\mathcal{Y}}}^t(\hat{x}, \tilde{y})) \quad (1.1)$$

with state vector $(\hat{x}, \tilde{y}) \in \mathcal{X} \times \tilde{\mathcal{Y}}$, surrogate resolved dynamics $\tilde{\Phi}_{\mathcal{X}}^t : \mathcal{X} \times \mathcal{Z} \rightarrow \mathcal{X}$, $\tilde{\Phi}_{\mathcal{X}}^t = \text{proj}_{\mathcal{X}} \circ \tilde{\Phi}$ and surrogate unresolved dynamics $\tilde{\Phi}_{\tilde{\mathcal{Y}}}^t : \mathcal{X} \times \tilde{\mathcal{Y}} \rightarrow \tilde{\mathcal{Y}}$, $\tilde{\Phi}_{\tilde{\mathcal{Y}}}^t = \text{proj}_{\tilde{\mathcal{Y}}} \circ \tilde{\Phi}$. To build the surrogate dynamics map $\tilde{\Phi}^t$ we need to define the surrogate space $\tilde{\mathcal{Y}}$, the surrogate flux map \tilde{Z} , and the surrogate dynamics maps $\tilde{\Phi}_{\mathcal{X}}^t$ and $\tilde{\Phi}_{\tilde{\mathcal{Y}}}^t$.

1.2. Main results. In this work we extend the original quantum mechanical closure framework (QMCL) to the case of spatiotemporal dynamics governed by partial differential equations. The QMCL framework models the unresolved variables of a dynamical system as a quantum mechanical system, using notions from quantum mechanics to define the surrogate flux map and surrogate dynamics [20, 16, 17]. We combine the original QMCL scheme with elements of the vector valued spectral analysis (VSA) framework introduced in [22] to develop a scheme that can effectively and efficiently model the closure of spatiotemporal dynamics. The main features of the present work can be summarized as follows.

1. *Positivity preservation.* As with the original QMCL work, our framework uses the noncommutative setting of operator algebras to encode the original classical dynamics, leading to a closure scheme that is positivity preserving. This means that positive flux terms in the original dynamics are represented

by positive operators in our closure model, producing positive surrogate flux terms. Generating surrogate fluxes that preserve the sign of the original fluxes is a nontrivial task and has important consequences for the closure of dynamics with sign definite quantities [17].

2. *Symmetry factorization.* Taking advantage of the symmetry factorization properties of the VSA framework, we derive a dynamical closure scheme that has important invariance properties under the actions of the spatial symmetry group of the original resolved dynamics. This enables us to form an especially compressed representation of the original spatiotemporal dynamics, leading to a data driven realization of our closure scheme that can be applied to complex dynamics with tractable computational cost [22].
3. *Computational efficiency.* In addition to the factorization of spatial symmetries, we implement the data driven formulation of our scheme in a way that lowers the cost of its most computationally expensive operations. As with the original QMCL and VSA frameworks, our data driven scheme requires solving an eigenvalue problem for a kernel matrix. In the setting of spatiotemporal dynamics, the dimensions of this matrix can be very large, making the eigenvalue problem one of the most expensive tasks in our scheme. To address that we perform a positivity preserving approximation of the kernel matrix by a lower rank matrix, and use the lower rank approximation to solve the eigenvalue problem with reduced cost [9, 40].
4. *Application.* We apply our scheme to a closure problem for the shallow water equations on a one dimensional spatial domain. The shallow water equations are a hyperbolic system of partial differential equations with important applications in fields such as water waves modeling and ocean dynamics [41, 42]. We demonstrate that our scheme can effectively capture and reproduce the main features of the dynamics, including for out of sample initial conditions.

1.3. Paper layout. In Section 2 we provide a brief overview of the original QMCL framework. In Section 3 we extend this framework to the closure of spatiotemporal dynamics. We present the main features of the extended scheme, the elements it borrows from the VSA framework, as well as its data driven realization. Next, in Section 4 we apply the extended scheme to a closure problem for the shallow water equations and present our numerical results. We conclude with a discussion of some aspects of the presented scheme and future work directions in Section 5. Appendix A provides additional details on the computational implementation of the data driven formulation of our closure scheme.

2. Quantum mechanical closure framework. In this section we provide a brief overview of QMCL as it has been developed in [20, 16, 17]. The core of the QMCL framework consists of two steps: (1) embedding the classical dynamics into an infinite dimensional quantum mechanical system; (2) projecting the infinite dimensional system to a finite dimensional subsystem. The infinite dimensional embedding of the classical dynamics is treated in Section 2.1. In Section 2.2 we present the process used to project the embedded dynamics to a finite dimensional subsystem and derive a closure model.

In the description of QMCL provided below we intentionally omit some of the details required for its precise description and implementation. A detailed treatment of the scheme, including its data driven realization, will be given in the following sections once we extend it to the closure of dynamics governed by partial differential equations. A detailed analysis of QMCL as presented below can be found in [20, 16,

17].

2.1. Infinite dimensional embedding. To build the quantum mechanical closure framework we start by embedding the classical dynamics on state space X into a quantum mechanical system on the infinite dimensional Hilbert space $H := L^2(X, \mu; \mathbb{R})$. This involves embedding observables (functions of state) and probability densities, as well as the evolution of said densities under the dynamics and their bayesian conditioning.

In the following we denote by $B(H)$ the space of bounded operators on Hilbert space H . We write $Q(H)$ to denote the space of quantum states on H , which are positive, trace class operators of unit trace. Note that positivity implies self adjointness in this context. Quantum states are also referred to as quantum density operators. In this work we mainly use pure quantum states, which are rank-1 quantum density operators and are equivalent to projections along a unit vector [23, 34, 36].

Every classical observable $f \in L^\infty(X, \mu; \mathbb{R}) \subset H$ is mapped to a self adjoint multiplication operator $A_f \in B(H)$, $A_f g = fg$ for all $g \in H$, referred to as a quantum observable. Additionally, every classical probability density $p \in L^1(X, \mu; \mathbb{R})$, $\sqrt{p} \in H$, is mapped to the quantum density operator $\rho_p \in Q(H)$, $\rho_p = \langle \sqrt{p}, \cdot \rangle \sqrt{p}$, representing a pure quantum state. The expected value of observable $A \in B(H)$ when the quantum system is in state $\rho \in Q(H)$ is given by $\mathbb{E}_\rho A = \text{tr}(\rho A) \in \mathbb{R}$, which is connected to the theory of quantum measurement [23, 34, 36].

We use the notion of quantum measurement to define the surrogate flux map $\tilde{Z} : \tilde{\mathcal{Y}} \rightarrow \mathcal{Z}$ needed for the evolution of the resolved dynamics. In particular using a quantum state $\rho \in Q(H)$ to model the state of the unresolved degrees of freedom, and a finite number of operators $A^{(j)} \in B(H)$, $j \in \{0, \dots, d-1\}$, to model $d \in \mathbb{N}$ observables of the system's unresolved state, we define each component of the surrogate flux map $\tilde{Z} : Q(H) \rightarrow \mathbb{R}^d$ as

$$\tilde{Z}^{(j)}(\rho) = \mathbb{E}_\rho(A^{(j)}) = \text{tr}(\rho A^{(j)}).$$

In other words we use flux space $\mathcal{Z} = \mathbb{R}^d$ and the space of quantum states $\tilde{\mathcal{Y}} = Q(H)$ to model the unresolved degrees of freedom of the dynamics.

In addition to evaluating the required flux terms we need to be able to evolve a quantum state under the system's dynamics and condition it based on observed dynamical behavior. In the classical case, the square root of probability densities $\sqrt{p} \in H$ evolves according to the unitary group of transfer operators, $P^n : H \rightarrow H$, $P^n \sqrt{p} = \sqrt{p} \circ \Phi^{-n}$, $n \in \mathbb{N}$. Accordingly, the evolution of quantum states $\rho \in Q(H)$ is governed by the induced transfer operator $\mathcal{P}^n : Q(H) \rightarrow Q(H)$, $\mathcal{P}^n \rho = P^n \rho P^{-n}$. In analogy to bayesian conditioning of classical probability densities, we can condition a quantum state $\rho \in Q(H)$ using a quantum effect operator $e \in B(H)$, $0 \leq e \leq \text{Id}$,

$$\rho|_e = \frac{\sqrt{e} \rho \sqrt{e}}{\mathbb{E}_\rho e}, \quad (2.1)$$

where \sqrt{e} denotes the positive square root of e . The above equation can be interpreted as the quantum analogue of the classical Bayes rule [17].

A quantum effect operator can be thought of as the quantum analogue of an indicator function used in classical probability to represent an event, namely a set in the event space. For instance, for a given set $B \subset X$ we can build the indicator function $1_B \in H$ taking the value one on B and zero elsewhere. The quantum effect operator $e_B \in B(H)$ can then be defined as multiplication by 1_B , namely $e_B f = 1_B f$ for all $f \in H$.

2.2. Closure modeling. We build a finite dimensional subspace $H^L \subset H$ using the leading L elements of an orthonormal basis $\{\phi_\ell\}_{\ell=0}^{L-1} \subset H$. To obtain such a basis we define a kernel integral operator $K : H \rightarrow H$

$$Kf = \int_X k(\cdot, x)f(x)d\mu(x)$$

using a symmetric kernel function $k \in L^2(X \times X, \mu \times \mu; \mathbb{R})$. Operator K is compact and self adjoint, so its eigenfunctions form an orthonormal basis of H . We define H^L as the linear span of its leading L eigenfunctions. Having built H^L , we project operators acting in H to operators acting in H^L . This is done for all operators needed for the quantum mechanical embedding of the original classical dynamics.

To build our closure modeling framework we set $\tilde{\mathcal{Y}} = Q(H^L)$; namely, we use quantum states to model the unresolved degrees of freedom of the surrogate dynamics $\tilde{\Phi}^t$ from (1.1). Having made that choice, we now describe the calculation of fluxes needed for evolving the resolved state under $\tilde{\Phi}_{\mathcal{X}}^t$, and the surrogate map $\tilde{\Phi}_{\mathcal{Y}}^t$ used to evolve the quantum state representing the unresolved state. To do so, we use a discrete time version of the above flow maps, denoting them by $\tilde{\Phi}_{\mathcal{X}}^{n\Delta t}$ and $\tilde{\Phi}_{\mathcal{Y}}^{n\Delta t}$ with $n \in \mathbb{N}$ and timestep $\Delta t > 0$.

Given the resolved system state $\hat{x}_i \in \mathcal{X}$ at timestep t_i , we want to compute state $\hat{x}_{i+1} = \tilde{\Phi}_{\mathcal{X}}(\hat{x}_i, \tilde{z}_i)$ using flux terms $\tilde{z}_i \in \mathcal{Z}$. We use $\mathcal{Z} = \mathbb{R}^d$ for some $d \in \mathbb{N}$; that is, \tilde{z} has components $\tilde{z}_i^{(j)} \in \mathbb{R}$, $j \in \{0, \dots, d-1\}$. To calculate the component fluxes we use a quantum state $\rho_i \in Q(H^L)$ representing the unresolved state at time t_i , and d quantum observables $A^{(j)} \in B(H^L)$. Each observable $A^{(j)}$ is a projected multiplication operator determined by the corresponding components $Z^{(j)}$ of the true flux function $Z : \mathcal{Y} \rightarrow \mathcal{Z}$. Intuitively, each $A^{(j)}$ represents the possible range of values of the corresponding true flux term $z^{(j)}$. Each surrogate flux term $\tilde{z}_i^{(j)}$ is computed as the expectation value of observable $A^{(j)}$ with respect to quantum state ρ_i

$$\tilde{z}_i^{(j)} = \tilde{Z}^{(j)}(\rho_i) = \mathbb{E}_{\rho_i}(A^{(j)}) = \text{tr}(\rho_i A^{(j)}).$$

The resolved state is then updated by $x_{i+1} = \tilde{\Phi}_{\mathcal{X}}^{\Delta t}(x_i, \tilde{z}_i)$.

Next we define the surrogate unresolved dynamics map $\tilde{\Phi}_{\mathcal{Y}}^{\Delta t}$ used to update the quantum state, $\rho_{i+1} = \tilde{\Phi}_{\mathcal{Y}}^{\Delta t}(\hat{x}_i, \rho_i)$. The quantum state update consists of two steps, a prediction and a correction step. Given the current quantum state ρ_i , we first use the projected transfer operator $\mathcal{P}_L : Q(H^L) \rightarrow Q(H^L)$ to compute the prior state

$$\rho'_{i+1} = \frac{\mathcal{P}_L \rho_i}{\text{tr}(\mathcal{P}_L \rho_i)}.$$

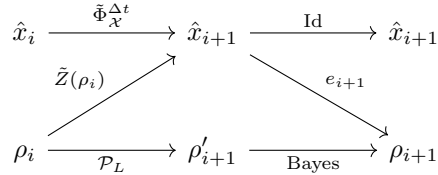
Renormalizing the quantum state after acting with \mathcal{P}_L is required because the projected operator \mathcal{P}_L is generally not unitary. Mapping $\rho_i \mapsto \rho'_{i+1}$ corresponds to the prediction step. The correction step involves using the updated resolved state \hat{x}_{i+1} to correct our prediction ρ'_{i+1} . To do so, we use state \hat{x}_{i+1} to build the projected quantum effect operator $e_{i+1} \in B(H^L)$. Using the quantum Bayes rule (2.1) we condition the prior state ρ'_{i+1} to compute the posterior state

$$\rho_{i+1} = \rho'_{i+1}|_{e_{i+1}} = \frac{\sqrt{e_{i+1}}\rho'_{i+1}\sqrt{e_{i+1}}}{\text{tr}(\sqrt{e_{i+1}}\rho'_{i+1}\sqrt{e_{i+1}})}.$$

The above two steps make up the surrogate unresolved dynamics $\tilde{\Phi}_{\mathcal{Y}}^{\Delta t}$. Although not unitary, operator \mathcal{P}_L is trace nonincreasing, which means that it can be interpreted

as governing the evolution of the open quantum system $H^L \subset H$. Under this light, the reduction of $\text{tr}(\rho)$ when acting with \mathcal{P}_L can be viewed as decoherence or leakage of density due to interaction with the environment [23, 34, 36].

The QMCL closure framework as developed above can be summarized in the following diagram, which depicts the evolution of the built surrogate dynamical system for one timestep [17].



In the diagram Id denotes the formal identity map.

3. Closure of partial differential equations. In this section we extend the QMCL scheme to the case of spatiotemporal dynamics governed by partial differential equations. One of the distinguishing features of the extended scheme is the appropriate handling of dynamical symmetries. We develop the extended scheme by pairing QMCL with the vector valued spectral analysis (VSA) framework [22], which combines methods from operator valued kernels and delay embedding to construct efficient compressed representations of dynamics in the presence of dynamical symmetries.

In Section 3.1 we define the appropriate function space H and describe the process of embedding the classical spatiotemporal dynamics into a quantum mechanical system in H . In Section 3.2 we introduce the kernel we use to discretize (compress) the embedded dynamics to a finite dimensional subsystem. In Sections 3.3 and 3.4 we explore the symmetry invariance properties of the derived eigenfunction basis and their consequences. In Sections 3.5 and 3.6 we develop the data driven formulation of the extended QMCL scheme which can be realized numerically.

3.1. Closure modeling. As explained in detail in Section 1.1, we consider spatiotemporal dynamics $\Phi^t : X \rightarrow X$, $t \geq 0$, possessing ergodic invariant measure μ with compact support, and infinite dimensional state space $X \subset L^2(S, \nu; \mathbb{R})$ where S denotes a spatial domain. We assume the state space decomposition $X = \mathcal{X} \times \mathcal{Y}$ where \mathcal{X} is the finite dimensional resolved state space and \mathcal{Y} the unresolved state space.

To provide a general definition of the resolved state space $\mathcal{X} \subset X$ we consider measure space (S, \mathcal{A}, ν) where \mathcal{A} denotes the Borel σ -algebra on S . We form the subalgebra $\mathcal{A}_M \subset \mathcal{A}$ generated by a finite collection of $M \in \mathbb{N}$ disjoint subsets $S_m \subset S$, $m \in \{0, \dots, M-1\}$, such that $\cup_{m=0}^{M-1} S_m = S$. Next we define measure ν_M as the restriction of ν to σ -algebra \mathcal{A}_M . The resolved state space is defined as the M -dimensional subspace $\mathcal{X} = L^2(S, \nu_M; \mathbb{R}) \cap X$. As a Hilbert space \mathcal{X} is isomorphic to \mathbb{R}^M with a scaled euclidean inner product. Each subset $S_m \subset S$ used to generate subalgebra \mathcal{A}_M can also be represented by its center point $s_m \in S_m$. We denote by $S_M = \{s_m\}_{m=0}^{M-1} \subset S$ the collection of those center points.

To embed the classical dynamics Φ^t we define the Hilbert space of vector valued observables $H = L^2(X, \mu; H_S)$ with $H_S = L^2(S, \nu_M; \mathbb{R})$. Introducing product state space $\Omega = X \times S$ and measure $\sigma = \mu \times \nu_M$ we define $H_\Omega = L^2(\Omega, \sigma; \mathbb{R})$ and note the following Hilbert space isomorphisms

$$H \simeq H_X \otimes H_S \simeq H_\Omega,$$

where $H_X = L^2(X, \mu; \mathbb{R})$. Namely, for every vector valued observable $\vec{f} \in H$ there is a corresponding real valued $f \in H_\Omega$ such that for almost every $x \in X$ and $s \in S$ $f(x, \cdot) = \vec{f}(x) \in H_S$ and $f(x, s) = \vec{f}(x)(s) \in \mathbb{R}$. The motivation for our choice of space H is our interest in observables that can effectively capture *spatiotemporal* dynamics; that is, patterns of evolution that have both a temporal dependence $x \in X$ and a spatial dependence $s \in S$. Given an observable $\vec{f} \in H$ the map $t \mapsto \vec{f}(\Phi^t(x))$ represents a spatiotemporal pattern generated by the dynamics Φ^t [22].

In the previous paragraph we abused notation slightly to write $\vec{f}(x)(s)$ for a function $\vec{f}(x) \in H_S$, when we formally mean $\int_S \vec{f}(x)(s) 1_{S_j} d\nu_M(s) / \nu_M(S_j)$ where subset $S_j \in \{S_m\}_{m=0}^{M-1} \subset S$ denotes one of the disjoint subsets used to define measure ν_M such that $s \in S_j$. Without misunderstanding, we will keep using this simplified notation throughout this work.

The definitions of quantum observables, quantum effects and the induced transfer operator carry over from Section 2 after using the new definition of Hilbert space H . Quantum states are now modeled as an operator valued field over S , $\rho \in L^2(S, \nu_M; B(H))$ with $\text{ran } \rho \subseteq Q(H) \subset B(H)$. This allows us to compute fluxes that vary over the spatial domain S for each quantum observable $A^{(j)} \in B(H)$, $j \in \{0, \dots, d-1\}$. More specifically, the surrogate flux map is defined as $\tilde{Z} : L^2(S, \nu_M; B(H)) \rightarrow L^2(S, \nu_M; \mathbb{R}^d)$ with action for each component

$$\tilde{Z}^{(j)}(\rho)(s) = \text{tr}(\rho(s)A^{(j)}) \in \mathbb{R}$$

where $\rho(s) \in Q(H) \subset B(H)$ denotes the quantum state representing point $s \in S$.

In the above construction we have made the space choices $\tilde{\mathcal{Y}} = L^2(S, \nu_M; B(H))$ and $\tilde{\mathcal{Z}} = L^2(S, \nu_M; \mathbb{R}^d)$. Namely, we use one quantum state to represent the unresolved degrees of freedom of the dynamics at each point in the spatial domain S , which in turn generate d flux terms at each spatial point using the quantum observables $A^{(j)}$.

Having embedded the original dynamics into an infinite dimensional quantum system in Hilbert space H , we now have to discretize space H using the eigendecomposition of a kernel integral operator. We tackle this task in the next section.

3.2. Choice of kernel. To build our closure scheme on H we use data generated from a dynamical trajectory $x_n = \Phi^{n\Delta t}(x_0)$, $x_0 \in X$, $n \in \mathbb{N}$, with sampling timestep $\Delta t > 0$. We do not require access to the full state samples $x_n \in X$; only to the corresponding resolved state samples $\hat{x}_n = \text{proj}_{\mathcal{X}}(x_n) \in \mathcal{X}$ and flux samples $z_n \in \mathcal{Z}$. Note that for each $n \in \mathbb{N}$, \hat{x}_n and z_n are functions on S , with $\hat{x}_n(s)$ and $z_n(s)$ denoting their values at point $s \in S$ of the spatial domain.

To discretize the space $H_\Omega \simeq H$ we use the orthonormal basis generated by the eigenfunctions of a kernel integral operator $K : H_\Omega \rightarrow H_\Omega$

$$Kf = \int_\Omega k(\cdot, \omega) f(\omega) d\sigma(\omega) \quad (3.1)$$

with a symmetric kernel $k \in L^2(\Omega \times \Omega, \sigma \times \sigma; \mathbb{R})$. By forming an operator acting directly on H_Ω we obtain eigenfunctions that are generally not of separable, tensor product form, and can thus represent dynamical patterns that are intrinsically spatiotemporal. This is in contrast to traditional approaches where one builds a basis for temporal space H_X , and then forms its tensor product with a basis for spatial space H_S to form a basis for $H_\Omega \simeq H_X \otimes H_S$ [22]. As we will see below, due to the presence of dynamical symmetries, our approach allows us to build a more compressed representation of the dynamics on H , meaning that each eigenfunction of operator K as defined above can represent more complicated spatiotemporal patterns.

To have a kernel function k that relies only on the sampled information we have access to, we employ data space \mathcal{W} and data map $W : \Omega \rightarrow \mathcal{W}$. We introduce data space kernel $k_w : \mathcal{W} \times \mathcal{W} \rightarrow \mathbb{R}$ and consider k as its pullback $k(\omega, \omega') = k_w(W(\omega), W(\omega'))$. In this work we use a kernel k_w that acts in delay coordinate space $\mathcal{W} = \mathbb{R}^Q$ where $Q \in \mathbb{N}$ denotes the number of delays. As explained in detail below, for each sample $\omega = (x, s) \in X \times S$ we embed the resolved state component $(\text{proj}_{\mathcal{X}}(x), s) \in \mathcal{X} \times S$ into \mathbb{R}^Q by using delays that act locally at spatial point $s \in S$. This allows us to recover some of the dynamical information lost when projecting to the resolved component of the state, as well as to factor redundancies introduced in the sampled data by dynamical symmetries [22].

Consider the data map $W_Q : \Omega \rightarrow \mathbb{R}^Q$

$$W_Q((x, s)) = (\text{proj}_{\mathcal{X}}(x)(s), \text{proj}_{\mathcal{X}}(\Phi^{-\Delta t}(x))(s), \dots, \text{proj}_{\mathcal{X}}(\Phi^{-(Q-1)\Delta t}(x))(s)) \quad (3.2)$$

which corresponds to S -pointwise delay embedding of product state sample $\omega = (x, s)$. Using this map we define the gaussian kernel function $k_w : \mathbb{R}^Q \times \mathbb{R}^Q \rightarrow \mathbb{R}$

$$k_w(W_Q(\omega), W_Q(\omega')) = \exp\left(-\frac{1}{\epsilon_Q} \|W_Q(\omega) - W_Q(\omega')\|_Q^2\right) \quad (3.3)$$

where $\|\cdot\|_Q$ denotes the 2-norm in \mathbb{R}^Q and $\epsilon > 0$ is a tunable bandwidth parameter. The parameter ϵ can be calibrated using the procedure developed in [12]. In our numerical experiments we normalize the above kernel to turn it into a bistochastic kernel. The bistochastic kernel normalization process and motivation for using it can be found in [11, 13].

With this choice of kernel function, we use the eigendecomposition of operator K from (3.1) to build an orthonormal basis for its range $\text{ran } K \subset H_\Omega$. We then use its L leading eigenfunctions to define the finite dimensional subspace H_Ω^L as their linear span. Once subspace H_Ω^L has been formed, we proceed to project all operators involved in QMCL from $B(H_\Omega)$ to $B(H_\Omega^L)$, which can be represented by finite dimensional matrices. This process will be developed in Section 3.5 along with the data driven realization of the extended closure scheme.

In the next section we describe the properties of the subspace $\text{ran } K \subset H_\Omega$ obtained through the eigendecomposition of K .

3.3. Dynamical symmetries. We consider a symmetry group G' acting on the spatial domain S by a continuous left action $\Gamma_{S,g} : S \rightarrow S, g \in G'$. As explained in Section 1.1 we assume that the dynamics Φ^t is equivariant under the actions of G'

$$\Gamma_{X,g} \circ \Phi^t = \Phi^t \circ \Gamma_{X,g}$$

for all $t \geq 0$ and $g \in G'$, where $\Gamma_{X,g}(x) = x \circ \Gamma_{S,g}^{-1}$ denotes the group's induced actions on state space X . Each action $\Gamma_{X,g}$ represents a dynamical symmetry of the dynamics Φ^t .

We consider the decomposition of dynamics Φ^t into its resolved $\Phi_{\mathcal{X}}^t$ and unresolved $\Phi_{\mathcal{Y}}^t$ components. In general, the coarsening process used to derive the resolved dynamics from the original one may lead to loss of some of the original symmetries. Accordingly, we focus on a subgroup $G \subseteq G'$ that corresponds to the set of symmetries obeyed by the resolved dynamics $\Phi_{\mathcal{X}}^t$. We define the induced action $\Gamma_{\mathcal{X},g} : \mathcal{X} \rightarrow \mathcal{X}$, $\Gamma_{\mathcal{X},g} = \text{proj}_{\mathcal{X}} \circ \Gamma_{X,g}$, $g \in G$, and assume that the resolved dynamics $\Phi_{\mathcal{X}}^t$ is equivariant

under the appropriate actions of G

$$\Gamma_{\mathcal{X},g} \circ \Phi_{\mathcal{X}}^t = \Phi_{\mathcal{X}}^t \circ \Gamma_{\mathcal{X},g} \quad (3.4)$$

for all $t \geq 0, g \in G$. From now on we focus on subgroup G and equivariance property (3.4). As explained below, our choice of kernel naturally exploits this equivariance property to bestow an analogous invariance property on the eigenfunctions of the kernel integral operator.

Under the action of data map W_Q from (3.2) the product space Ω can be viewed as a topological fiber bundle (Ω, B_Q, W_Q) , where Ω is the total space, $B_Q = W_Q(\Omega)$ the base space, and $W_Q : \Omega \rightarrow B_Q$ the continuous projection map. The fibers are equivalence classes $[\omega]_Q = W_Q^{-1}(b) \subseteq \Omega, b \in B_Q$, defined as the set of values on which W_Q is constant [22]. For our choice of projection map W_Q , each fiber consists of points in Ω whose resolved dynamical evolution over Q delays is identical.

Using the group action $\Gamma_{\Omega,g} : \Omega \rightarrow \Omega, \Gamma_{\Omega,g} = \Gamma_{\mathcal{X},g} \otimes \Gamma_{\mathcal{S},g}$ we define the G -orbit of $\omega \in \Omega$ as the set $\Gamma_{\Omega}(\omega) = \{\Gamma_{\Omega,g}(\omega) : g \in G\}$. As shown in [22], $\Gamma_{\Omega}(\omega) \subseteq [\omega]_Q$ for all $\omega \in \Omega$; that is, every fiber $[\omega]_Q$ includes the symmetric transformations of ω induced by group G .

Because kernel function k in (3.1) acts by composition with projection map $W_Q, k = k_w \circ (W_Q \times W_Q)$, it is constant on the $[\cdot]_Q$ fibers by construction [22]. As a result, every function $f \in \text{ran } K$ is constant on the fibers; namely, $f(\omega') = f(\omega)$ for all $\omega' \in [\omega]_Q$. Given that G -orbits $\Gamma_{\Omega}(\omega) \subseteq [\omega]_Q$ for all $\omega \in \Omega$, it follows that functions $f \in \text{ran } K$ satisfy the invariance property

$$f \circ \Gamma_{\Omega,g} = f \quad (3.5)$$

for all $g \in G$. In particular this implies that all eigenfunctions of integral operator K corresponding to nonzero eigenvalues satisfy this property as well. Combined with the fact that all $f \in \text{ran } K$ are continuous by continuity of k , we conclude that $\text{ran } K$ consists entirely of continuous functions that are constant on the fibers $[\cdot]_Q$.

Note that due to the continuity of $f \in \text{ran } K$, any such function is well defined in a pointwise sense. As a result, we do not need to assume that action $\Gamma_{\Omega,g}$ preserves the σ -null sets to form the composition $f \circ \Gamma_{\Omega,g}$ used in (3.5).

To gain additional insight into the properties of $\text{ran } K$ we define the induced action $\Gamma_{H_{\Omega},g} : \text{ran } K \subset H_{\Omega} \rightarrow H_{\Omega}, \Gamma_{H_{\Omega},g} f = f \circ \Gamma_{\Omega,g}^{-1}, g \in G$. From (3.5) we immediately conclude that $\Gamma_{H_{\Omega},g} f = f$ for all $f \in \text{ran } K, g \in G$; namely, $\Gamma_{H_{\Omega},g} K = K$. This means that our choice of kernel factors the symmetry group actions $\Gamma_{H_{\Omega},g}$ from $\text{ran } K$. As a result, by using the eigenfunctions of K corresponding to nonzero eigenvalues we derive a basis of $\text{ran } K$ that is invariant under the actions of G , instead of getting multiple ‘‘copies’’ of the same underlying functions generated by the action of different $g \in G$. Most importantly for our purposes, this means that fewer eigenfunctions are needed to represent complex spatiotemporal dynamics, thereby producing a more efficient compression of the dynamics in H_{Ω} to subspace H_{Ω}^L [22].

3.4. Representation of fluxes. As explained in the previous section all functions $f \in H_{\Omega}$ that can be represented by our basis spanning $\text{ran } K \subset H_{\Omega}$ must satisfy the invariance property (3.5). In this section we study the representation of flux functions with respect to this basis.

As stated in (3.4) we assume that the resolved dynamics $\Phi_{\mathcal{X}}^t$ is equivariant under the induced actions of symmetry group G . Dynamics $\Phi_{\mathcal{X}}^t$ can be considered as the formal exponential of generating differential operator $V_{\mathcal{X}} : \mathcal{X} \times \mathcal{Z} \rightarrow T\mathcal{X}$ which governs

the resolved dynamics, where $T\mathcal{X}$ denotes the tangent bundle of \mathcal{X} . Informally $V_{\mathcal{X}}$ can be thought of as the operator representing the right hand side of the partial differential equation modeling the resolved dynamics.

Based on a choice of flux terms we decompose $V_{\mathcal{X}} = V_{\mathcal{X}\mathcal{X}} + V_{\mathcal{X}\mathcal{Z}}$, with $V_{\mathcal{X}\mathcal{X}} : \mathcal{X} \rightarrow T\mathcal{X}$ acting on the resolved state only and $V_{\mathcal{X}\mathcal{Z}} : \mathcal{X} \times \mathcal{Z} \rightarrow T\mathcal{X}$ acting on both resolved and unresolved state to generate the required flux terms. Operators $V_{\mathcal{X}\mathcal{X}}$ and $V_{\mathcal{X}\mathcal{Z}}$ are generated by the associated vector fields $v_{\mathcal{X}\mathcal{X}}$ and $v_{\mathcal{X}\mathcal{Z}}$ acting on the differentiable manifold \mathcal{X} .

Even though operator $V_{\mathcal{X}}$ is equivariant under the action of G , there is no guarantee that each of $V_{\mathcal{X}\mathcal{X}}$ and $V_{\mathcal{X}\mathcal{Z}}$ is *independently* equivariant under G . How to decompose $V_{\mathcal{X}}$ into its two components is a design choice, and not all choices will lead to components obeying the same set of symmetries. For this reason we make the additional assumption that operator $V_{\mathcal{X}\mathcal{Z}}$ is equivariant under the associated actions of symmetry group G

$$\Gamma_{T\mathcal{X},g} \circ V_{\mathcal{X}\mathcal{Z}} = V_{\mathcal{X}\mathcal{Z}} \circ (\Gamma_{\mathcal{X},g} \times \Gamma_{\mathcal{Z},g})$$

for all $g \in G$ with $\Gamma_{T\mathcal{X},g} : T\mathcal{X} \rightarrow T\mathcal{X}$ and $\Gamma_{\mathcal{Z},g} : \mathcal{Z} \rightarrow \mathcal{Z}$ denoting the actions of G on $T\mathcal{X}$ and \mathcal{Z} . Under this assumption all flux functions involved in our closure model satisfy the invariance property (3.5) and can thus be represented by our eigenfunction basis.

3.5. Data driven formulation. In this section we use the framework developed in the previous sections to define a data driven closure scheme that can be realized numerically. We first establish the data driven formulation using one dynamical trajectory to generate our training data. In the next section we extend this to the case of training data consisting of multiple trajectories.

We consider a finite dynamical trajectory of $N \in \mathbb{N}$ samples $X_N = \{x_n\}_{n=0}^{N-1} \subset X$ with $x_n = \Phi^{n\Delta t}(x_0)$, $x_0 \in X$, $\Delta t > 0$. We define the discrete sampling measure $\mu_N = \sum_{n=0}^{N-1} \delta_{x_n}/N$ and corresponding finite dimensional Hilbert space $H_{X,N} = L^2(X, \mu_N; \mathbb{R})$, where functions are represented by their values on samples $X_N \subset X$. Combining the above we define the associated product space $H_{\Omega,N} = L^2(\Omega, \sigma_N; \mathbb{R})$ with discrete product measure $\sigma_N = \mu_N \times \nu_M$.

We assume that the sampling measures μ_N converge to the invariant measure μ in the weak-* topology of finite Borel measures on the support of μ as $N \rightarrow \infty$. We refer the reader to [16, 17] for details on the convergence properties of the QMCL scheme in the limit of large training data $N \rightarrow \infty$.

As before we do not assume access to the dynamical trajectory samples x_n but only to the resolved state samples $\hat{x}_n = \text{proj}_{\mathcal{X}}(x_n) \in \mathcal{X}$ and flux samples $z_n \in \mathcal{Z}$. We denote the state samples in product form by $\omega_{nm} = (x_n, s_m) \in \Omega$ with state $x_n \in X_N$ and gridpoint $s_m \in S_M$.

Using the data space kernel k_w of (3.3) we define the associated data driven kernel integral operator $K_N : H_{\Omega,N} \rightarrow H_{\Omega,N}$

$$\begin{aligned} K_N f &= \int_{\Omega} k_w(W_Q(\cdot), W_Q(\omega)) f(\omega) d\sigma_N(\omega) \\ &= \frac{1}{NM} \sum_{n=0}^{N-1} \sum_{m=0}^{M-1} k_w(W_Q(\cdot), W_Q(\omega_{nm})) f(\omega_{nm}). \end{aligned} \tag{3.6}$$

Using the L leading eigenfunctions $\{\phi_\ell\}_{\ell=0}^{L-1}$ of K_N we construct the L -dimensional subspace $H_{\Omega,N}^L \subset H_{\Omega,N}$ as their linear span. In what follows we make use of the

orthogonal projection $\text{proj}_L : H_{\Omega,N} \rightarrow H_{\Omega,N}$, $\text{ran proj}_L = H_{\Omega,N}^L$. Using proj_L an operator $A \in B(H_{\Omega,N})$ can be projected by conjugation $\text{Proj}_L A = \text{proj}_L A \text{proj}_L \in B(H_{\Omega,N}^L)$. Note that the latter projection preserves positivity; namely, $\text{Proj}_L A$ is a positive operator whenever A is positive.

In the data driven scheme, quantum observables are self adjoint operators in $B(H_{\Omega,N}^L)$. To construct such an observable A we first define a multiplication operator $M_f \in B(H_{\Omega,N})$, $M_f g = fg$ for all $g \in H_{\Omega,N}$, where $f(\omega_{nm}) = z_n(s_m)$ corresponds to the training flux samples $z_n \in \mathcal{Z}$ viewed as a function in $H_{\Omega,N}$. Orthogonal projection then yields $A = \text{Proj}_L M_f \in B(H_{\Omega,N}^L)$. Note that after projection A is generally no longer a multiplication operator. Using the orthonormal basis $\{\phi_\ell\}_{\ell=0}^{L-1}$ each operator $A \in B(H_{\Omega,N}^L)$ is represented by a matrix $\mathbf{A} \in \mathbb{R}^{L \times L}$ with entries $A_{ij} = \langle \phi_i, A \phi_j \rangle_N$. In this way for any $g \in H_{\Omega,N}^L$ the operation Ag is represented by $\mathbf{A}g$, with coefficient vector $g \in \mathbb{R}^L$, $g_\ell = \langle \phi_\ell, g \rangle_N$. One of the distinguishing features of the discretization process employed in QMCL is that if the flux samples z_n used to build observable A are positive, then A is a positive operator that will produce positive surrogate fluxes [17].

Quantum states form a field $\rho \in L^2(S, \nu_M; B(H_{\Omega,N}^L))$ with one quantum state $\rho_m = \rho(s_m) \in Q(H_{\Omega,N}^L) \subset B(H_{\Omega,N}^L)$ for each gridpoint $s_m \in S_M$. In this work we focus on pure quantum states, namely rank-1 quantum density operators acting as projections along a given vector. For a gridpoint $s_m \in S_M$, quantum state ρ_m is constructed as the projection along a function $h_m \in H_{\Omega,N}^L$, $\rho_m = \langle h_m, \cdot \rangle_N h_m$. As such, we represent each state ρ_m by the coefficient vector $\underline{\rho}_m \in \mathbb{R}^L$, $\rho_{m,\ell} = \langle \phi_\ell, h_m \rangle_N$. This is equivalent to representing ρ_m by the matrix $\boldsymbol{\rho}_m \in \mathbb{R}^{L \times L}$, $\rho_{m,ij} = \langle \phi_i, \rho_m \phi_j \rangle_N$ but leads to savings in memory and computation [17].

The surrogate flux map $\tilde{Z} : L^2(S, \nu_M; B(H_{\Omega,N}^L)) \rightarrow L^2(S, \nu_M; \mathbb{R}^d)$ maps the operator field $\rho \in L^2(S, \nu_M; B(H_{\Omega,N}^L))$ to the flux field $\tilde{z} \in L^2(S, \nu_M; \mathbb{R}^d)$, $d \in \mathbb{N}$, where each vector of the latter corresponds to the computed surrogate flux values for each sampled gridpoint. More specifically, given d quantum observables $A^{(j)} \in B(H_{\Omega,N}^L)$, $j \in \{0, \dots, d-1\}$, and a quantum state field $\rho \in L^2(S, \nu_M; B(H_{\Omega,N}^L))$, each component of the flux map \tilde{Z} acts by $\tilde{Z}^{(j)}(\rho)(s_m) = \text{tr}(\rho(s_m)A^{(j)}) \in \mathbb{R}$. By slightly abusing notation we may write more compactly $\tilde{z}_m^{(j)} = \tilde{Z}^{(j)}(\rho_m) = \text{tr}(\rho_m A^{(j)})$. Using our basis representation of each $A^{(j)}$ by matrix $\mathbf{A}^{(j)} \in \mathbb{R}^{L \times L}$ and ρ_m by vector $\underline{\rho}_m \in \mathbb{R}^L$, we have that $\tilde{z}_m^{(j)} = \underline{\rho}_m^T \mathbf{A}^{(j)} \underline{\rho}_m \in \mathbb{R}$ where superscript T denotes transposition.

The induced transfer operator is defined as $\mathcal{P}_N^L : B(H_{\Omega,N}^L) \rightarrow B(H_{\Omega,N}^L)$. Because we work with pure quantum states, which can be represented by vectors instead of matrices, it is sufficient to approximate transfer operator $P_N^L : H_{\Omega,N}^L \rightarrow H_{\Omega,N}^L$ instead of \mathcal{P}_N^L . To build P_N^L we begin by approximating $P_N : H_{\Omega,N} \rightarrow H_{\Omega,N}$ by the shift operator $\hat{P}_N : H_{\Omega,N} \rightarrow H_{\Omega,N}$

$$\hat{P}_N f(\hat{x}_n, s_m) = \begin{cases} f(\hat{x}_{n+1}, s_m) & \text{if } 0 \leq n < N-1 \\ 0 & \text{if } n = N-1. \end{cases}$$

After projection we obtain $P_N^L = \text{Proj}_L \hat{P}_N$ represented by a matrix $\mathbf{P}_N^L \in \mathbb{R}^{L \times L}$, $(P_N^L)_{ij} = \langle \phi_i, P_N^L \phi_j \rangle_N$. Given a single quantum state $\rho_i \in Q(H_{\Omega,N}^L)$ at timestep t_i with vector representation $\underline{\rho}_i \in \mathbb{R}^L$, we obtain the updated state $\underline{\rho}_{i+1}$ by

$$\underline{\rho}_{i+1} = \frac{(\mathbf{P}_N^L)^T \underline{\rho}_i}{\|(\mathbf{P}_N^L)^T \underline{\rho}_i\|_2}$$

where superscript T denotes transposition. Matrix \mathbf{P}_N^L is in general not unitary, which is why we renormalize the updated quantum state after applying \mathbf{P}_N^L .

Quantum effects are operators $e \in B(H_{\Omega,N}^L)$ used to condition quantum density states based on a given state vector $\omega \in \Omega$. To build effect e from state vector ω we introduce kernel function $k_c : \Omega \times \Omega \rightarrow \mathbb{R}$, defined as the pullback of kernel $k_{cw} : \mathcal{W}_c \times \mathcal{W}_c \rightarrow \mathbb{R}$, $k_c(\omega, \omega') = k_{cw}(W_c(\omega), W_c(\omega'))$ with data space \mathcal{W}_c and associated data map $W_c : \Omega \rightarrow \mathcal{W}_c$. To define kernel function k_{cw} we define the data space $\mathcal{W}_c = \mathbb{R}^J$ with parameter $J \in \mathbb{N}$. For a given gridpoint $s_m \in S_M$ and state vector $\omega_m = (x, s_m) \in \Omega$ we define the action of data map $W_J : \Omega \rightarrow \mathbb{R}^J$ as

$$W_J((x, s_m)) = (\text{proj}_{\mathcal{X}}(x)(s_{m-(J-1)/2}), \dots, \text{proj}_{\mathcal{X}}(x)(s_m), \dots, \text{proj}_{\mathcal{X}}(x)(s_{m+(J-1)/2})).$$

The kernel $k_{cw} : \mathbb{R}^J \times \mathbb{R}^J \rightarrow \mathbb{R}$ is then defined as

$$k_{cw}(W_J(\omega), W_J(\omega')) = \exp\left(-\frac{1}{\epsilon' J} \|W_J(\omega) - W_J(\omega')\|_J^2\right) \quad (3.7)$$

with $\|\cdot\|_J$ the 2-norm in \mathbb{R}^J and $\epsilon' > 0$ a bandwidth parameter. Note that the bandwidth parameter ϵ' is different from the one introduced earlier in kernel (3.3); it can again be selected using the tuning procedure developed in [12]. In our numerical experiments we employ the above kernel using a variable bandwidth function; details on the bandwidth function and an algorithm for computing it can be found in [4, 19].

For a fixed gridpoint $s_m \in S_M$, given a state vector ω_m and the full training dataset $\{\omega_{nm}\}_{nm=0}^{NM-1}$, kernel k_c is used to produce function $f_m \in H_{\Omega,N}$, $f_m(\cdot) = k_c(\omega_m, \cdot)$, leading to multiplication operator M_{f_m} and the desired quantum effect $e_m = \text{Proj}_L M_{f_m}$. Employing the quantum Bayes rule (2.1) then yields the conditioned quantum state $\rho_m|_{e_m}$ for gridpoint s_m . Intuitively, function f_m can be thought of as an affinity function on state space Ω , measuring how “similar” the given state ω_m is to the states included in our training dataset. Building operator e_m and conditioning the prior state ρ_m then yields the posterior state $\rho_m|_{e_m}$ that encodes the state space affinities captured by f_m . We often refer to f_m as the *feature vector* produced by kernel k_c for product state vector ω_m .

With respect to our basis representation of ρ_m by vector $\underline{\rho}_m \in \mathbb{R}^L$ and effect e_m by matrix $\mathbf{e}_m \in \mathbb{R}^{L \times L}$, the conditioning operation takes the form

$$\rho_m|_{e_m} = \frac{\sqrt{\mathbf{e}_m} \underline{\rho}_m}{\|\sqrt{\mathbf{e}_m} \underline{\rho}_m\|_2}.$$

To avoid having to compute the square root of matrix \mathbf{e}_m , we modify the way we form effect e_m . We use function $f_m^{1/2} \in H_{\Omega,N}$ to form multiplication operator $\tilde{A}_m = M_{f_m^{1/2}}$ and define effect $\tilde{e}_m = (\text{Proj}_L \tilde{A}_m)^2 = (\tilde{A}_m^L)^2$. Conditioning with respect to \tilde{e}_m now takes the form

$$\rho_m|_{\tilde{e}_m} = \frac{\sqrt{\tilde{\mathbf{e}}_m} \underline{\rho}_m}{\|\sqrt{\tilde{\mathbf{e}}_m} \underline{\rho}_m\|_2} = \frac{\tilde{\mathbf{A}}_m^L \underline{\rho}_m}{\|\tilde{\mathbf{A}}_m^L \underline{\rho}_m\|_2}.$$

Although effects \tilde{e}_m and e_m are generally different, the two are equal when $L = N$, and thus also share the same asymptotic limit as $N \rightarrow \infty$ and $L \rightarrow \infty$ [17].

The data map W_J embeds state vector $(x, s_m) \in \Omega$ into \mathbb{R}^J by considering the resolved state values at gridpoints neighboring $s_m \in S_M$, mimicking the structure of

the stencil used for the spatial discretization of the considered dynamics. In this way kernel k_{cw} compares the stencil of values around s_m to the corresponding stencil of points for every state included in our training data. This makes for a stronger affinity condition than comparing values of states at only a single gridpoint. For hyperbolic partial differential equations, where the notion of a local propagation velocity is well defined, using a stencil of values is analogous to using a time delayed signal with a generally fractional number of delays.

Because the spatially local value $\omega_m = (x, s_m)$ is compared to every other state vector present in our training data $\{\omega_{nm}\}_{nm=0}^{NM-1}$, spatial translations of state x are naturally factored during the conditioning process. This means that if a spatial translation of state x is present in our training dataset, then the similarity between product state $\omega_m = (x, s_m)$ and the corresponding value of the spatial translation of state x will be identified in the conditioning process. For partial differential equations with spatial translation symmetry, this means that we do not have to artificially inflate our training dataset by including all spatial translations of the sampled states.

3.6. Multitrajectory data. To build the data driven formulation of the scheme we have so far relied on a single dynamical trajectory $x_n = \Phi^{n\Delta t}(x_0)$, $x_0 \in X$. In this section we generalize this construction to the case where our training data consists of multiple trajectories.

We consider $K \in \mathbb{N}$ trajectories of N_k samples each, denoted by $\{x_n^{(k)}\}_{n=0}^{N_k-1}$, $k \in \{0, \dots, K-1\}$. Considering each trajectory independently we use the approach outlined in Section 3.5 to build an orthonormal basis for the Hilbert space H_{Ω, N_k} , which is the space of functions represented by their values on the samples of the k th trajectory only. We use the L_k leading eigenfunctions $\{\phi_\ell^{(k)}\}_{\ell=0}^{L_k-1}$ to define subspace $H_{\Omega, N_k}^{L_k} \subset H_{\Omega, N_k}$. Denoting $N = \sum_{k=0}^{K-1} N_k$ and $L = \sum_{k=0}^{K-1} L_k$ we define the combined space

$$H_{\Omega, N}^L = H_{\Omega, N_0}^{L_0} \oplus \dots \oplus H_{\Omega, N_{K-1}}^{L_{K-1}},$$

with the direct sum of the individual bases producing a basis for the combined space $H_{\Omega, N}^L$. The basis derived in this way consists of a total of L eigenfunctions, each representing the values of the function on N samples. For each eigenfunction, all of its values are zero except for the block of values that corresponds to the N_k samples of the k th trajectory it was derived from.

Having derived the basis for space $H_{\Omega, N}^L$, the construction of the rest of the scheme proceeds as in Section 3.5. The only additional difference is in the approximation of the transfer operator P_N by the shift operator \hat{P}_N , where time shifts are now applied only *within* each trajectory, and the last temporal sample of each trajectory is mapped to zero. Namely, we make sure not to shift samples *across* different trajectories.

Using a single dynamical trajectory is generally sufficient when considering a dynamical system possessing a unique physical measure, namely a measure that can be sampled by a set of initial conditions of positive measure with respect to the ambient measure. These are measures whose sampling can be realized numerically, with SRB measures being an important example [43]. In such systems, a single long trajectory can be used to sample the physical measure of the dynamics.

Using multiple trajectories as training data is of interest when considering dynamical systems possessing multiple physical measures. For instance, hamiltonian systems or hyperbolic systems with several competing basins of attraction. Additionally, using multiple trajectories is necessary in parametric forecasting, where one considers a dynamical system whose qualitative dynamics changes with respect to a

bifurcation parameter.

Finally, even in systems with a unique physical measure, being able to use multiple trajectories to sample that measure allows one to consider optimal sampling strategies. In designing such a strategy, one tries to optimize the sampling rate with respect to a chosen objective, instead of relying on the inherent rate provided by a single dynamical trajectory.

4. Application. The shallow water equations govern the evolution of a fluid when its vertical length scale can be considered negligible compared to its horizontal length scale. The equations are derived from the conservation laws for mass and momentum. Various forms of the equations have applications in areas such as ocean fluid dynamics, often incorporating additional terms modeling the effects of bottom topography and Coriolis force [41, 42].

We consider the shallow water equations on the one dimensional spatial domain $S = [-L_S/2, L_S/2]$ with periodic boundary conditions. The system of equations governs the evolution of water height $h(t, \cdot)$ and momentum $q(t, \cdot) = h(t, \cdot)v(t, \cdot)$, with $v(t, \cdot)$ denoting the velocity field and $t \geq 0$ time. The scalar fields h and q are assumed to take values in a sufficiently regular subset of $L^2(S, \nu; \mathbb{R})$. The governing equations read

$$\begin{aligned} \partial_t h + \partial_s q &= 0 \\ \partial_t q + \partial_s (q^2/h + 1/2Fr^{-2}h^2) &= 0 \end{aligned} \tag{4.1}$$

subject to an appropriate initial condition. In the above ∂_t and ∂_s denote differentiation with respect to time and space respectively; Fr denotes the flow's Froude number, which is a dimensionless ratio of inertial over gravitational forces. Using the state variable $x = (h, q) \in X \subset L^2(S, \nu; \mathbb{R}^2)$ and function $f(x) = (q, q^2/h + 1/2Fr^{-2}h^2)$ we rewrite (4.1) in the compact form

$$\partial_t x + \partial_s f(x) = 0. \tag{4.2}$$

The dynamics governed by (4.2) is equivariant under the actions of the spatial translation group on S .

We define the total energy of the fluid as the sum of its kinetic and potential energies

$$E(t) = \frac{1}{2} \int_S q^2(t, s)/h(t, s) d\nu(s) + \frac{1}{2} Fr^{-2} \int_S h^2(t, s) d\nu(s)$$

for all $t \geq 0$. If one assumes that the height and velocity fields are differentiable for all $t \geq 0$, thereby excluding discontinuous solutions, then total energy is conserved along solution trajectories, namely $dE(t)/dt = 0$. In this case the state space can be decomposed into the dynamics invariant disjoint subsets

$$\mathcal{E}_c := \{x \in X : E(t) = c \text{ for all } t \geq 0\}$$

each one defined as the subset of constant energy $c \geq 0$.

In the formation of discontinuities, the internal energy of the fluid is increased across a discontinuity, accompanied by an increase in entropy. Since the above definition of total energy does not include internal energy, total energy is decreased across a discontinuity [42]. In the present work we consider only differentiable solutions.

4.1. Discretization. We employ a finite volume spatial discretization of (4.2) using a uniform fine grid of $M_f \in \mathbb{N}$ cells with length $\Delta s = L/M_f$ each, centered at points $s_m \in S$, $m \in \{0, \dots, M_f - 1\}$. We denote $S_f = \{s_m\}_{m=0}^{M_f-1} \subset M$ and

$C_m = [s_m - \Delta s/2, s_m + \Delta s/2] \subset S$, $m \in \{0, \dots, M_f - 1\}$. Each cell C_m can also be represented by its center point $s_m \in S_f$. We define the cell averaged state variable

$$x(t, s) = \frac{1}{\Delta s} \int_{s_m - \Delta s/2}^{s_m + \Delta s/2} x(t, s) d\nu(s), \quad s \in C_m$$

reusing the same state symbol x . For any $t \geq 0$ function $x(t, \cdot)$ can be represented by vector $\underline{x} \in \mathbb{R}^{2M_f}$ with $x_m = x(t, s_m)$, $s_m \in C_m$.

We derive the semidiscretized system of equations

$$\dot{x}_m = \frac{1}{\Delta s} (F_m - F_{m+1}) \quad (4.3)$$

using the local Lax-Friedrich (LLF) numerical flux

$$F_m = \frac{1}{2} [f(x_{m-1}) + f(x_m)] - \frac{\lambda_m}{2} (x_m - x_{m-1}) \quad (4.4)$$

with

$$\lambda_m = \max(|q_{m-1}/h_{m-1}| + Fr^{-1}\sqrt{h_{m-1}}, |q_m/h_m| + Fr^{-1}\sqrt{h_m}), \quad (4.5)$$

where subscripts denote components of the associated vectors. In the above F_m denotes the numerical flux at the left face of cell C_m [25]. Based on (4.4) and (4.5) we define the formal map \mathcal{F}_{LLF}

$$F_m = \mathcal{F}_{LLF}(x_{m-1}, x_m).$$

We now form a coarse grid and associated coarse variables defined as local spatial averages of the fine variables x_m . In particular we form $M_c \in \mathbb{N}$ coarse grid cells by merging every $M_s \in \mathbb{N}$ fine cells; in this way, $M_c = M_f/M_s$ and each coarse cell has length $\Delta \hat{s} = M_s \Delta s$. We define the resulting coarse grid $S_c = \{\hat{s}_m\}_{m=0}^{M_c-1} \subset S$ and cells $\hat{C}_m = [\hat{s}_m - \Delta \hat{s}/2, \hat{s}_m + \Delta \hat{s}/2] \subset S$, $m \in \{0, \dots, M_c - 1\}$. The coarse grid state variable \hat{x} is formed using spatial averages over each coarse cell

$$\hat{x}(t, s) = \frac{1}{M_s} \sum_{j=M_s m}^{M_s(m+1)-1} x_j, \quad s \in \hat{C}_m.$$

For the evolution of the coarse state variable \hat{x} we derive the system of equations

$$\dot{\hat{x}}_m = \frac{1}{\Delta \hat{s}} [(\hat{F}_m + G_m) - (\hat{F}_{m+1} + G_{m+1})] \quad (4.6)$$

with coarse grid fluxes

$$\hat{F}_m := \mathcal{F}_{LLF}(\hat{x}_{m-1}, \hat{x}_m) \quad (4.7)$$

and subgrid fluxes

$$G_m := F_{M_s m} - \hat{F}_m. \quad (4.8)$$

The system (4.6) is equivariant under the actions of the discrete group of spatial translations on S_c .

By definition, the coarse grid fluxes (4.7) depend only on the coarse variables. On the contrary, the subgrid fluxes (4.8) depend on both the coarse and the original fine variables; in particular, they depend on the values of x_m in the fine cells that border the interfaces of each coarse cell. The subgrid fluxes act as antidiffusive corrections to

the coarse grid fluxes, increasing the accuracy of the discretization compared to one performed entirely on the coarse grid [39].

The temporal discretization of evolution equations (4.3) and (4.6) is carried out using the modified Euler method (two-stage Runge-Kutta), which has favorable structure preservation properties for the present problem [39]. In what follows we consider the coarse mesh variables as the resolved degrees of freedom and the discrete time version of (4.6) as the true resolved dynamics. For the system to be complete we need to provide a closure model that can infer the subgrid fluxes G_m from the resolved variables \hat{x}_m , thereby removing the explicit dependence on the fine mesh variables x_m .

4.2. Closure model. To define the appropriate state space X for the dynamics we begin by considering the measure space (S, \mathcal{A}, ν) where \mathcal{A} denotes the Borel σ -algebra on the spatial domain S . We form $\mathcal{A}_f \subset \mathcal{A}$ as the σ -algebra generated by the disjoint subsets $C_m \subset S$ that correspond to the fine discretization cells; analogously, we form $\mathcal{A}_c \subset \mathcal{A}$ as the σ -algebra generated by the coarse cells $\hat{C}_m \subset S$. We define measures ν_f and ν_c as the restrictions of ν to the σ -algebras \mathcal{A}_f and \mathcal{A}_c respectively.

The state space of the true spatiotemporal dynamics (4.2) is an infinite dimensional Hilbert space $X \subset L^2(S, \nu; \mathbb{R}^2)$. To be able to simulate the “true” dynamics numerically we approximate the full state space $X \subset L^2(S, \nu_f; \mathbb{R}^2)$ by a Hilbert subspace of the space of L^2 functions on the mesh produced by our fine discretization. Next we define the resolved state space $\mathcal{X} = L^2(S, \nu_c; \mathbb{R}^2) \cap X$ and decompose the full state space as $X = \mathcal{X} \oplus \mathcal{Y}$ with unresolved state space $\mathcal{Y} = \mathcal{X}^\perp$. In this way the resolved state space can be considered as the space of piecewise constant functions, each taking a constant value on each cell formed by the coarse discretization. We set flux space $\mathcal{Z} = L^2(S, \nu_c; \mathbb{R}^2)$ and true flux map $Z : \mathcal{Y} \rightarrow \mathcal{Z}$ with action given by (4.8). Now the full dynamics $\Phi^{n\Delta t} : X \rightarrow X$ is given by the discrete time version of (4.3) and the resolved dynamics $\Phi_{\mathcal{X}}^{n\Delta t} : \mathcal{X} \times \mathcal{Y} \rightarrow \mathcal{X}$ by the discrete time version of (4.6), with $n \in \mathbb{N}$ and timesteps $\Delta t > 0$ and $\Delta \hat{t} = M_s \Delta t$.

Using the full dynamics we generate N samples of the resolved state $\{\hat{x}_n\}_{n=0}^{N-1} \subset \mathcal{X}$ and fluxes $\{z_n\}_{n=0}^{N-1} \subset \mathcal{Z}$ which may consist of one or more dynamical trajectories. Each sample \hat{x}_n or z_n is represented by a vector in \mathbb{R}^{2M_c} holding the values corresponding to the height h and momentum q variables in each coarse grid cell. We define the product state space $\Omega := X \times S$ and associated Hilbert space $H_{\Omega, N} := L^2(\Omega, \sigma_N; \mathbb{R})$ with $\sigma_N = \mu_N \times \nu_M$ and $\nu_M = \nu_c$. For notational consistency with the previous sections, in the following we denote by $M = M_c$ the number of coarse grid cells and by $S_M = S_c \subset S$ the set of grid points representing the coarse grid cells.

To form our closure model we define the surrogate unresolved state space $\tilde{\mathcal{Y}} = L^2(S, \nu_M; B(H_\Omega))$ with associated surrogate flux map $\tilde{Z} : \tilde{\mathcal{Y}} \rightarrow \mathcal{Z}$ and surrogate resolved dynamics $\tilde{\Phi}_{\mathcal{X}}^{n\Delta t} : \mathcal{X} \times \tilde{\mathcal{Y}} \rightarrow \mathcal{X}$. To define the action of the surrogate flux map \tilde{Z} we introduce two quantum observables $A^{(j)} \in B(H_{\Omega, N})$, $j \in \{0, 1\}$. Observable $A^{(0)}$ will be used to produce the flux values for the height h variables; observable $A^{(1)}$ the flux values for the momentum q variables. With these choices, the fluxes for the h variables are computed as $\tilde{z}^{(0)}(s_m) = \text{tr}(\rho(s_m)A^{(0)})$ and those for the q variables as $\tilde{z}^{(1)}(s_m) = \text{tr}(\rho(s_m)A^{(1)})$, $s_m \in S_M$.

In Appendix A we explain the sequence of steps used to build the QMCL scheme and apply it to predict the dynamics based on a given initial condition.

4.3. Numerical results. We consider the shallow water equations (4.2) on the spatial domain $S = [-50, 50]$ with Froude number $Fr = 1/\sqrt{2g}$ and g denoting the

acceleration of gravity. We perform the spatial discretization using a fine grid of $M_f = 1920$ cells and the temporal discretization using the midpoint Euler method and a timestep $\Delta t = 0.1\Delta s$ where Δs is the length of each fine cell.

Training. We define the one-parameter family of initial conditions

$$\begin{aligned} h_0(s) &= 1 + 0.3(1 - \delta/2) \sin\left(\frac{2\pi}{L_S} 3.5(1 - \delta/2)s + \pi/6\right) \\ v_0(s) &= 1 + 0.2(1 - \delta) \sin\left(\frac{2\pi}{L_S} 3(1 - \delta)s\right) \end{aligned} \tag{4.9}$$

with $s \in S$, $L_S = 100$, parameter $0 \leq \delta \leq 1$, h_0 the initial condition for height and $q_0 = h_0 v_0$ the initial condition for momentum. Our training data consists of three trajectories generated using the values $\delta \in \{0, 0.5, 1\}$. For each trajectory we integrate the full dynamics (4.3) in time for 12,200 timesteps and then sample the next 3,260 timesteps. Each sample contains the values of functions h and q on the fine grid.

To derive the resolved state samples that will be used as our training data, we coarsen the model and above sampled data. By averaging the sampled data over every $M_s = 20$ fine cells we arrive at a coarse grid of $M = 96$ cells of length $\Delta \hat{s} = 20\Delta s$ each. Given that each cell is now 20 times longer we also increase the sampling timestep by the same amount to set $\Delta \hat{t} = 20\Delta t$. From the original 3,260 samples per trajectory generated on the fine grid we keep every 20th sample, leading to 163 samples per trajectory. For each one of those samples we spatially average the solution over every 20 cells to derive our resolved state samples, namely the averaged values of h and q over the coarse grid. We then derive the subgrid flux training samples using (4.8).

Using $Q = 64$ delays, these samples yield 100 training samples per trajectory in delay embedded form, adding up to $N = 300$ samples in total. Each resolved state sample consists of $2M = 192$ values, 96 for each of the height and momentum variables. With this training dataset, the dimension of the product Hilbert space $H_{\Omega, N}$ is equal to $NM = 28800$. Using the approach described in Section 3.6 for dealing with multitrajectory training data, we build an orthonormal basis using a total of $L = 6144$ eigenfunctions and define $H_{\Omega, N}^L$ as their linear span. Each eigenfunction is represented by a vector in \mathbb{R}^{NM} . Finally, we set $J = 5$ to define data map W_J that will be used for the bayesian conditioning of quantum states.

To form the orthonormal basis we must compute the eigenvectors of an $NM \times NM$ symmetric kernel matrix \mathbf{K}_N representing the data driven integral operator (3.6). To reduce the computational cost of this operation we perform a partial Cholesky factorization of \mathbf{K}_N to approximate it by lower rank matrix $\tilde{\mathbf{K}}_N = \mathbf{F}\mathbf{F}^T$ with $\mathbf{F} \in \mathbb{R}^{NM \times r}$ and $r < NM$. We perform the factorization using rank parameter $r = L = 6144$ and the randomized algorithm developed in [9]. We then use the approximate kernel matrix to perform its bistochastic normalization and solve the eigenvalue problem with reduced cost [40].

Prediction. To test the predictive performance of the QMCL scheme we use two initial conditions obtained from (4.9) for $\delta \in \{0.25, 0.75\}$, which are trajectories not included in the training dataset. After integrating the true dynamics (4.3) for 12,200 timesteps we spatially average the found solutions to generate the initial conditions that will be used to initialize the resolved state in QMCL. Using those initial conditions we integrate in time the coarse dynamics (4.6) using timestep $\Delta \hat{t}$ and the subgrid fluxes predicted by QMCL. In what follows we present results obtained after integrating for a total of 120 timesteps while performing bayesian conditioning of the quantum states every 10 timesteps.

The results comparing the evolution under the true and surrogate dynamics are grouped into four figures. Figures 1 and 3 include the results for the trajectory generated by the initial condition obtained from (4.9) for $\delta = 0.25$. Figures 2 and 4 showcase the results obtained for $\delta = 0.75$.

Looking at the heatmaps for the height and momentum fields in Figure 1 for the trajectory with $\delta = 0.25$ and Figure 2 for the one with $\delta = 0.75$, we see that QMCL clearly captures the main features of the dynamics for the tested time horizon. For both trajectories, QMCL correctly predicts the main traveling wave features of the dynamics, including the spatial variations of the waves as they interact with one another. Moreover, the magnitude of the predicted fields is consistent with the true dynamics in most regions of the spatial domain. In addition to the results shown in these figures, we have also verified that QMCL can reproduce the dynamical trajectories included in its training dataset with good accuracy.

In the present closure model, the subgrid fluxes play the role of antidiffusive corrections to the fluxes generated entirely on the coarse grid [39]. Their values are proportional to the spatial derivative of the associated field, taking large values when the height or momentum field is changing rapidly in space, and approximately zero value when the fields are constant in space. As a result, the contribution of the subgrid fluxes is critical in regions of large spatial variation of the height and momentum fields, counterbalancing the increased diffusion of the solution introduced by our coarsening of the original dynamics by spatial averaging. This implies that when the exact value of the subgrid fluxes is not predicted correctly by QMCL, the surrogate evolution will be more diffusive than the true evolution.

This effect can be seen in the heatmaps for the two trajectories. By comparing the true and predicted fields of height and momentum, we see that the surrogate dynamics leads to stronger diffusion of the solution in areas where there is strong spatial variation. The increased diffusion is seen in the plots as bleeding of color between different space-time regions, with the boundaries between those regions being less sharp than in the true dynamics. Similarly, the same effect can be seen by comparing the subgrid flux fields for height and momentum. In the true dynamics, the peaks of the fluxes are sharp and clearly separated from the valleys, with clearly visible waves traveling in opposite directions. In the predicted dynamics, although the waves are still predicted correctly, their peaks are not as sharp, with their values diffusing more strongly to the surrounding region.

The flux plots also clearly demonstrate the effect of bayesian conditioning, which for these results is performed every 10 timesteps. One can see the discontinuities that occur every 10 timesteps for the predicted fluxes over large regions of the spatial domain. These discontinuities represent corrections introduced to the predicted flux values every time conditioning of the quantum states is performed.

Similar conclusions can be drawn from the spatial profiles shown in Figure 3 for the trajectory with $\delta = 0.25$ and Figure 4 for that with $\delta = 0.75$. In these plots one can see that the subgrid fluxes are proportional to the spatial derivative of the associated field, leading to sharp variations in space. The predicted dynamics preserves the main features of the evolved fields, but struggles to capture the sharp peaks of the subgrid fluxes, leading to stronger diffusion of the height and momentum fields in regions of strong spatial variation.

4.4. Discussion. In QMCL the surrogate fluxes are computed as the expected value of an observable with respect to a given quantum state. As a result, to compute fluxes that vary strongly over the spatial domain one has to ensure that the used

quantum states are very *sharp*: obtaining a clear maximum in some regions of product space Ω and being close to zero everywhere else, formally similar to a finite sum of delta Dirac measures. Working with such sharp quantum states has both theoretical and numerical challenges.

Theoretically, producing accurate but very sharp quantum states requires a very precise choice of bandwidth parameter ϵ' used in kernel (3.7) for bayesian conditioning. Having such a selective kernel means that the resulting quantum state leads to highly accurate fluxes when the correct part of the training dataset is identified as similar to the current resolved state. However, it can lead to strongly inaccurate fluxes when regions of the training dataset are misidentified as similar, compared to using a less selective kernel that leads to wider averaging of the employed quantum observable.

Numerically, working with a very selective kernel can lead to numerical instability, especially when no region of the training dataset is identified as similar to the current observed dynamics. When that happens, the produced feature vector is approximately zero everywhere. During bayesian conditioning, this leads to a quantum state that is also approximately zero everywhere, making it numerically unstable to attempt to normalize that quantum state to unit norm. Working with a wider, less selective kernel makes this scenario less likely to occur, albeit with the tradeoff of less informative conditioning and thus less accurate predicted fluxes.

In addition to numerical instability, even if a very sharp quantum state can be consistently obtained by using a very selective kernel, there still remains the challenge of representing this quantum state with respect to the eigenfunction basis. Resolving such fine features usually requires a large number of eigenfunctions, leading to expensive simulations. Given that most QMCL operators are represented numerically as $L \times L$ matrices, the overall simulation cost scales with L^2 .

5. Conclusion. We have developed a framework for the dynamical closure of spatiotemporal dynamics which combines elements of the quantum mechanical framework developed in [20, 16, 17] and the vector valued spectral analysis (VSA) framework of [22]. We have shown that the present extended framework inherits the symmetry factorization properties of VSA during the basis construction process, and can also be used with training data consisting of multiple dynamical trajectories. Additionally, as with the original QMCL work, the process of embedding classical dynamics into the noncommutative setting of quantum mechanics leads to positivity preserving discretizations of classical observables and probability density functions [17].

We have applied QMCL to a closure problem for the shallow water equations on a periodic, one dimensional domain. The numerical results demonstrate that QMCL can correctly predict the dynamics of the out of sample initial conditions tested in this work, generating height and momentum fields that agree both qualitatively and quantitatively with the true data. At the same time, it struggles to fully capture the strong spatial variations observed in the subgrid fluxes, leading to more diffusive evolution. Overall, we believe that the results act as a successful proof of concept for the extension of QMCL to spatiotemporal dynamics, especially given the modest amount of data used for its training. Everything else kept the same, it is expected that increasing the amount of training data or the spectral resolution L will lead to improved prediction accuracy.

5.1. Computational aspects. Extending the QMCL framework to spatiotemporal dynamics comes with the challenge of increased computational cost for its implementation, primarily due to the increased size of the training datasets required to capture the main features of dynamics that evolves over both space and time. As

such, one key area of focus for future work is reducing the cost of implementation of QMCL and improving its scaling with sampling parameter N , spatial grid size M and spectral resolution parameter L .

In the offline stage the most expensive operation is computing the leading L eigenfunctions of the $NM \times NM$ symmetric kernel matrix \mathbf{K}_N representing kernel integral operator (3.6). Even for moderate size parameters N and M , solving such an eigenvalue problem can quickly become very expensive. As explained in Section 4.3 to reduce this computational cost when generating our numerical results we performed a partial Cholesky factorization of \mathbf{K}_N to approximate it by a lower rank matrix. The fact that the partial Cholesky factorization preserves the positivity of matrix entries means that we can use the approximate kernel matrix to perform its bistochastic normalization and solve the resulting eigenvalue problem with reduced cost [9, 40].

As an alternative we also tried using the random Fourier features (RFF) method to approximate \mathbf{K}_N by a lower rank matrix [31]. However, unlike the partial Cholesky factorization, the RFF method does not preserve positivity of matrix entries, which means that attempting to normalize the resulting approximate matrix is not a well defined operation. Additionally, we empirically found that a relatively large number of Fourier features was required to obtain a satisfactory approximation of kernel matrix \mathbf{K}_N compared to the rank parameter r required for the partial Cholesky factorization. We intend to continue investigating ways of reducing the cost of computing the kernel eigenfunction basis.

In the online stage the most expensive operation is the quantum state conditioning; more specifically, building the quantum effect operator from the current resolved state. To form the quantum effect operator we use kernel (3.7) to compare the current resolved state vector to all state vectors present in our training dataset. This is the only online operation that scales with the size of the training dataset NM , and requires that we have the training data loaded in memory throughout the online stage.

One way of alleviating this issue is to use the RFF method to approximate the out of sample evaluation of kernel (3.7), thereby eliminating the dependence on the training data [31, 21]. In our case this approach requires keeping in memory one $L \times L$ matrix for each random Fourier feature used. Namely, using r Fourier features requires holding in memory rL^2 floating point numbers of the employed precision. In our experiments we have found that a large number of Fourier features was required to resolve the fine spatial features of our state vectors, rendering this memory cost requirement unsustainable.

Another approach is to form a reduced representation of the training dataset and use that to form the quantum effect operator. For instance one could choose a subset of the original training dataset and rely only on that subset to perform the quantum state conditioning. The formation of that subset can be carried out using the kernel sampling algorithm that underlies the partial Cholesky factorization algorithms [9]. Our goal is to continue investigating these and similar directions for improving the performance of the quantum state conditioning operation.

A source of potential numerical instability in the implementation of QMCL is the renormalization of the quantum state after its bayesian conditioning. As briefly discussed in Section 4.4, this can become problematic when no part of the training dataset is identified by the conditioning kernel as being similar to the current resolved state, leading to an approximately zero feature vector and conditioned state. More generally, obtaining an approximately zero conditioned quantum state can happen when the prior quantum state and the observation encoded in the feature vector have

disjoint supports. One potential way of addressing this issue is resetting the prior quantum state to an uninformative state and repeating the conditioning operation. This requires erasing the historical information accumulated in the prior state, thereby placing a higher level of trust on the dynamical relevance of the observation. Building a better theoretical understanding of the conditions under which such a scenario might occur and the computational ways in which it can be addressed is a topic of future work.

Finally, the successful application of QMCL relies on the precise calibration of kernel bandwidth ϵ , number of delays Q and conditioning stencil size J . Having efficient, reliable algorithms for selecting these parameters based on a training dataset is very important. Tuning bandwidth parameter ϵ can be achieved reliably using the algorithm developed in [12], although corrections are usually required when working with small training datasets. When applicable, choosing the number of delays Q can be informed by the dimension of the attracting state space region sampled by the dynamical trajectories generating the training data [35]. However, such dimension estimates are rarely available for real world datasets and their underlying dynamics. It would be interesting to consider computational algorithms that can estimate the right range of values for Q based on the given training dataset, potentially also accounting for the presence of noise [45, 26, 6].

5.2. Theoretical aspects. One of the distinguishing features of the QMCL framework is that the classical dynamics is first embedded into the noncommutative setting of operator algebras used in quantum mechanics, and only then discretized to finite dimension. Namely, instead of directly discretizing functions on Hilbert space H to obtain functions on finite dimensional subspace H^L , we first map functions on H to operators in $B(H)$ and then discretize them to obtain operators in finite dimensional $B(H^L)$. This process renders the discretization employed by QMCL positivity preserving, with positive classical observables and probability density functions mapped to positive operators [17].

In addition to structure preserving properties, this discretization process embeds the discretized quantities in a space of larger dimension than direct discretization. More specifically, direct discretization maps real functions on H to functions on the L -dimensional subspace H^L . The QMCL discretization maps real functions on H to self adjoint real operators in $B(H^L)$, which is a subspace of dimension $\frac{1}{2}L(L+1)$. It would be interesting to explore whether this difference in dimension along with the noncommutative nature of $B(H^L)$ allow QMCL to encode more information about the original dynamics compared to closure schemes performed in H^L . Using tools from control theory and information theory one should be able to quantify the differences between the two discretization approaches and their consequences for downstream closure schemes.

Appendix A. Implementation details. The process of building and using the developed QMCL scheme to simulate the surrogate dynamics consists of two stages: the offline and online stages. Below we outline the steps followed in each stage.

Offline stage. The offline stage consists of the operations needed to build the QMCL scheme using the training data $\{\hat{x}_n\}_{n=0}^{N-1} \subset \mathcal{X}$ and $\{z_n\}_{n=0}^{N-1} \subset \mathcal{Z}$. This involves the following sequence of steps.

1. Using the resolved state samples $\{\hat{x}_n\}_{n=0}^{N-1}$ we calibrate the bandwidth parameter ϵ for kernel (3.3) and perform its bistochastic normalization.
2. We use samples $\{\hat{x}_n\}_{n=0}^{N-1}$ to compute the leading L eigenfunctions $\{\phi_\ell\}_{\ell=0}^{L-1}$

of integral operator (3.6), defining subspace $H_{\Omega,N}^L$ as their linear span. The eigenfunction basis is represented by matrix $\Phi \in \mathbb{R}^{NM \times L}$ holding one eigenfunction in each column.

3. We form the transfer operator P_N^L and represent it by matrix $\mathbf{P}_N^L \in \mathbb{R}^{L \times L}$.
4. We use the flux samples $\{z_n\}_{n=0}^{N-1}$ to form two quantum observables and project them to operators $A^{(0)}, A^{(1)} \in B(H_{\Omega,N}^L)$ represented by matrices $\mathbf{A}^{(0)}, \mathbf{A}^{(1)} \in \mathbb{R}^{L \times L}$. The first observable is built using the flux samples for the height h variables; the second using those for the momentum q variables.
5. We define the discrete field of quantum states $\rho \in L^2(S, \nu_M; B(H_{\Omega,N}^L))$ with one state corresponding to each coarse grid cell. Each quantum state $\rho_m = \rho(s_m) \in Q(H_{\Omega,N}^L) \subset B(H_{\Omega,N}^L)$, $s_m \in S_M$, is represented by a vector $\underline{\rho}_m \in \mathbb{R}^L$.
6. Using the resolved state samples $\{\hat{x}_n\}_{n=0}^{N-1}$ we calibrate the bandwidth parameter ϵ' of kernel (3.7) and compute the bandwidth function needed for its variable bandwidth generalization.

Online stage. In the online stage we use the operators built in the offline stage to timestep the surrogate dynamics. We denote by $\hat{x} \in \mathcal{X}$ and $\hat{z} \in \mathcal{Z}$ the resolved state and fluxes predicted by QMCL; this is to distinguish them from the true resolved state \hat{x} and fluxes z . The online stage consists of the following steps.

1. We initialize the resolved state \tilde{x} .
2. We initialize the quantum states representing each grid cell using an uninformative initial condition: each quantum state is set to the projection along the unit function $1_\Omega \in H_{\Omega,N}^L$ that takes the value 1 everywhere.
3. We condition each quantum state using the initial resolved state \tilde{x} and training data $\{\hat{x}_n\}_{n=0}^{N-1}$.
4. We use the quantum states and quantum observables to compute the discrete field of flux values \tilde{z} corresponding to two flux values for each grid cell.
5. We begin the timestepping loop.
 - (a) We update the resolved state using the computed fluxes.
 - (b) We update the quantum states using the transfer operator.
 - (c) We condition the quantum states using the updated resolved state and training data samples.
 - (d) We compute the updated flux values.

In the timestepping loop as presented above, the quantum states are conditioned at every timestep. In our presented numerical results we have instead elected to condition the states less frequently, by only performing bayesian conditioning every N_r timesteps with parameter $N_r \in \mathbb{N}$.

REFERENCES

- [1] A. ARAKAWA AND W. H. SCHUBERT, *Interaction of a cumulus cloud ensemble with the large-scale environment, Part I*, J. Atmos. Sci., 31 (1974), pp. 674–701.
- [2] J. BERNER, U. ACHATZ, L. BATTÉ, L. BENGTTSSON, A. D. L. CÁMARA, H. M. CHRISTENSEN, M. COLANGELI, D. R. B. COLEMAN, D. CROMMELIN, S. I. DOLAPTCHEV, C. L. E. FRANZKE, P. FRIEDERICHS, P. IMKELLER, H. JÄRVINEN, S. JURICKE, V. KITSIOS, F. LOTT, V. LUCARINI, S. MAHAJAN, T. N. PALMER, C. PENLAND, M. SAKRADZHA, J.-S. VON STORCH, A. WEISHEIMER, M. WENIGER, P. D. WILLIAMS, AND J.-I. YANO, *Stochastic parameterization: toward a new view of weather and climate models*, Bull. Amer. Meteor. Soc., 98 (2017), pp. 565–588.
- [3] T. BERRY, D. GIANNAKIS, AND J. HARLIM, *Bridging data science and dynamical systems theory*, Notices Amer. Math. Soc., 67 (2020), pp. 1336–1349.
- [4] T. BERRY AND J. HARLIM, *Variable bandwidth diffusion kernels*, Appl. Comput. Harmon. Anal.,

- 40 (2016), pp. 68–96.
- [5] K. BHATTACHARYA, B. HOSSEINI, N. B. KOVACHKI, AND A. M. STUART, *Model reduction and neural networks for parametric pdes*, SMAI J. Comput. Math., 7 (2021), pp. 121–157.
 - [6] J. BOTVINICK-GREENHOUSE, M. OPREA, R. MAULIK, AND Y. YANG, *Measure-theoretic time-delay embedding*, arXiv:2409.08768, (2024).
 - [7] K. CHAMPION, B. LUSCH, J. N. KUTZ, AND S. L. BRUNTON, *Data-driven discovery of coordinates and governing equations*, Proc. Natl. Acad. Sci. USA, 116 (2019), pp. 22445–22451.
 - [8] A.-T. G. CHARALAMPOPOULOS AND T. P. SAPSIS, *Machine-learning energy-preserving non-local closures for turbulent fluid flows and inertial tracers*, Phys. Rev. Fluids, 7 (2022), p. 024305.
 - [9] Y. CHEN, E. N. EPPERLY, J. A. TROPP, AND R. J. WEBBER, *Randomly pivoted Cholesky: practical approximation of a kernel matrix with few entry evaluations*, Comm. Pure Appl. Math., 78 (2024), pp. 995–1041.
 - [10] A. J. CHORIN AND F. LU, *Discrete approach to stochastic parametrization and dimension reduction in nonlinear dynamics*, Proc. Natl. Acad. Sci. USA, 112 (2015), pp. 9804–9809.
 - [11] R. R. COIFMAN AND M. J. HIRN, *Bi-stochastic kernels via asymmetric affinity functions*, Appl. Comput. Harmon. Anal., 35 (2013), pp. 177–180.
 - [12] R. R. COIFMAN, Y. SHKOLNISKY, F. J. SIGWORTH, AND A. SINGER, *Graph laplacian tomography from unknown random projections*, IEEE Trans. Image Process., 17 (2008), pp. 1891–1899.
 - [13] S. DAS, D. GIANNAKIS, AND J. SLAWINSKA, *Reproducing kernel Hilbert space compactification of unitary evolution groups*, Appl. Comput. Harmon. Anal., 54 (2021), pp. 75–136.
 - [14] W. E, *Principles of multiscale modeling*, Cambridge University Press, New York, 2011.
 - [15] W. E, E. ENGQUIST, X. LI, W. REN, AND E. VANDEN-EIJNDEN, *Heterogeneous multiscale methods: a review*, Commun. Comput. Phys., 2 (2007), pp. 367–450.
 - [16] D. FREEMAN, D. GIANNAKIS, B. MINTZ, A. OURMAZD, AND J. SLAWINSKA, *Data assimilation in operator algebras*, Proc. Natl. Acad. Sci. USA, 120 (2023), p. e2211115120.
 - [17] D. C. FREEMAN, D. GIANNAKIS, AND J. SLAWINSKA, *Quantum mechanics for closure of dynamical systems*, SIAM Multiscale Model. Simul., 22 (2024), pp. 283–333.
 - [18] P. R. GENT AND J. C. MCWILLIAMS, *Isopycnal mixing in ocean circulation models*, J. Phys. Oceanogr., 20 (1989), pp. 150–155.
 - [19] D. GIANNAKIS, *Data-driven spectral decomposition and forecasting of ergodic dynamical systems*, Appl. Comput. Harmon. Anal., 47 (2019), pp. 338–396.
 - [20] D. GIANNAKIS, *Quantum mechanics and data assimilation*, Phys. Rev. E, 100 (2019), p. 032207.
 - [21] D. GIANNAKIS, A. HENRIKSEN, J. A. TROPP, AND R. WARD, *Learning to forecast dynamical systems from streaming data*, SIAM J. Appl. Dyn. Syst., 22 (2023), pp. 527–558.
 - [22] D. GIANNAKIS, A. OURMAZD, J. SLAWINSKA, AND Z. ZHAO, *Spatiotemporal pattern extraction by spectral analysis of vector-valued observables*, J. Nonlinear Sci., 29 (2019), pp. 2385–2445.
 - [23] B. C. HALL, *Quantum theory for mathematicians*, Springer, New York, 2013.
 - [24] S. KLUS, F. NÜSKE, P. KOLTAI, H. WU, I. KEVREKIDIS, C. SCHÜTTE, AND F. NOÉ, *Data-driven model reduction and transfer operator approximation*, J. Nonlinear Sci., 28 (2018), pp. 985–1010.
 - [25] R. J. LEVEQUE, *Finite volume methods for hyperbolic problems*, Cambridge University Press, New York, 2002.
 - [26] N. MARWAN, M. C. ROMANO, M. THIEL, AND J. KURTHS, *Recurrence plots for the analysis of complex systems*, Phys. Rep., 438 (2007), pp. 237–329.
 - [27] T. N. PALMER, *A nonlinear dynamical perspective on model error: a proposal for non-local stochastic-dynamic parametrization in weather and climate prediction models*, Quart. J. Roy. Meteorol. Soc., 127 (2001), pp. 279–304.
 - [28] S. PAN AND K. DURAISAMY, *Data-driven of closure models*, SIAM J. Appl. Dyn. Syst., 17 (2018), pp. 2381–2413.
 - [29] G. A. PAVLIOTIS AND A. M. STUART, *Multiscale methods*, Springer, New York, 2008.
 - [30] D. QI AND J. HARLIM, *Machine learning-based statistical closure models for turbulent dynamical systems*, Philos. Trans. Roy. Soc. A, 380 (2022), p. 20210205.
 - [31] A. RAHIMI AND B. RECHT, *Random features for large-scale kernel machines*, in Advances in Neural Information Processing Systems, vol. 20, Curran Associates, 2007, pp. 1177–1184.
 - [32] M. RAISSI, P. PERDIKARIS, AND G. E. KARNIADAKIS, *Physics-informed neural networks: a deep learning framework for solving forward and inverse problems involving nonlinear partial differential equations*, J. Comput. Phys., 387 (2019), pp. 686–707.
 - [33] P. SAGAUT, *Large eddy simulation for incompressible flows*, Springer, Berlin, 2006.
 - [34] J. J. SAKURAI AND J. NAPOLITANO, *Modern quantum mechanics*, Cambridge University Press, Cambridge, 3rd ed., 2021.
 - [35] T. SAUER, J. A. YORKE, AND M. CASDAGLI, *Embedology*, J. Stat. Phys., 65 (1991), pp. 579–616.

- [36] L. A. TAKHTAJAN, *Quantum mechanics for mathematicians*, AMS, Providence, 2008.
- [37] R. TEMAM, *Infinite-dimensional dynamical systems in mechanics and physics*, Springer, New York, 2nd ed., 1997.
- [38] H. TENNEKES AND J. L. LUMLEY, *A first course in turbulence*, MIT Press, Cambridge, 1972.
- [39] I. TIMOFEYEV, A. SCHWARZMANN, AND D. KUZMIN, *Application of machine learning and convex limiting to subgrid flux modeling in the shallow-water equations*, arXiv:2407.17214, (2025).
- [40] C. VALES AND D. GIANNAKIS, *Eigenvalue decomposition of normalized kernel matrices by positivity preserving approximation*, In preparation.
- [41] G. K. VALLIS, *Atmospheric and oceanic fluid dynamics*, Cambridge University Press, Cambridge, 2nd ed., 2017.
- [42] G. B. WHITHAM, *Linear and nonlinear waves*, Wiley, New York, 1999.
- [43] L.-S. YOUNG, *What are SRB measures, and which dynamical systems have them?*, J. Stat. Phys., 108 (2002), pp. 733–754.
- [44] J. YUVAL AND P. A. O’GORMANN, *Stable machine-learning parameterization of subgrid processes for climate modeling at a range of resolutions*, Nat. Commun., 11 (2020), p. 3295.
- [45] J. P. ZBILUT AND C. L. WEBBER, *Embeddings and delays as derived from quantification of recurrence plots*, Phys. Lett. A, 171 (1992), pp. 199–203.

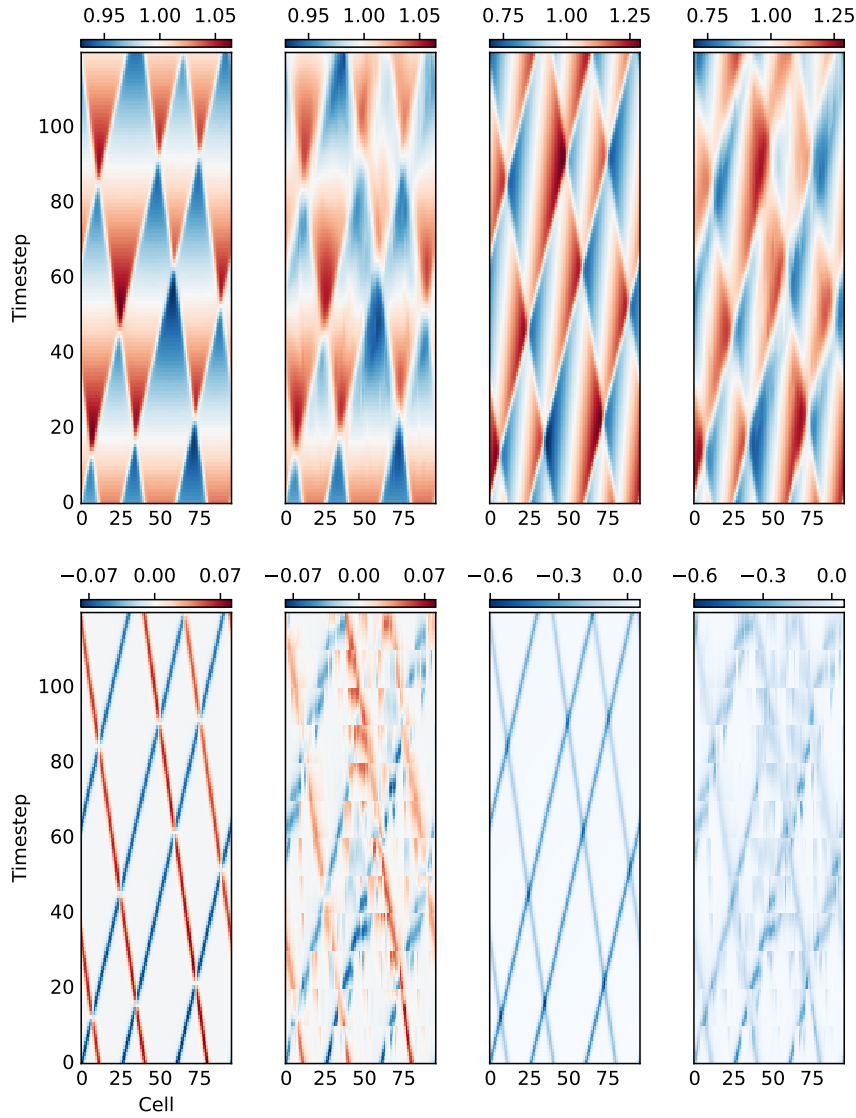


FIG. 1. Space-time heatmaps for trajectory with $\delta = 0.25$. Top row is the results for the resolved state variables; bottom row for the subgrid fluxes. For each row, from left to right: the first two plots show the results for the height field h , with the true results on the left and the predicted results on the right; the next two plots are the results for the momentum field q , with true results on the left and predicted on the right.

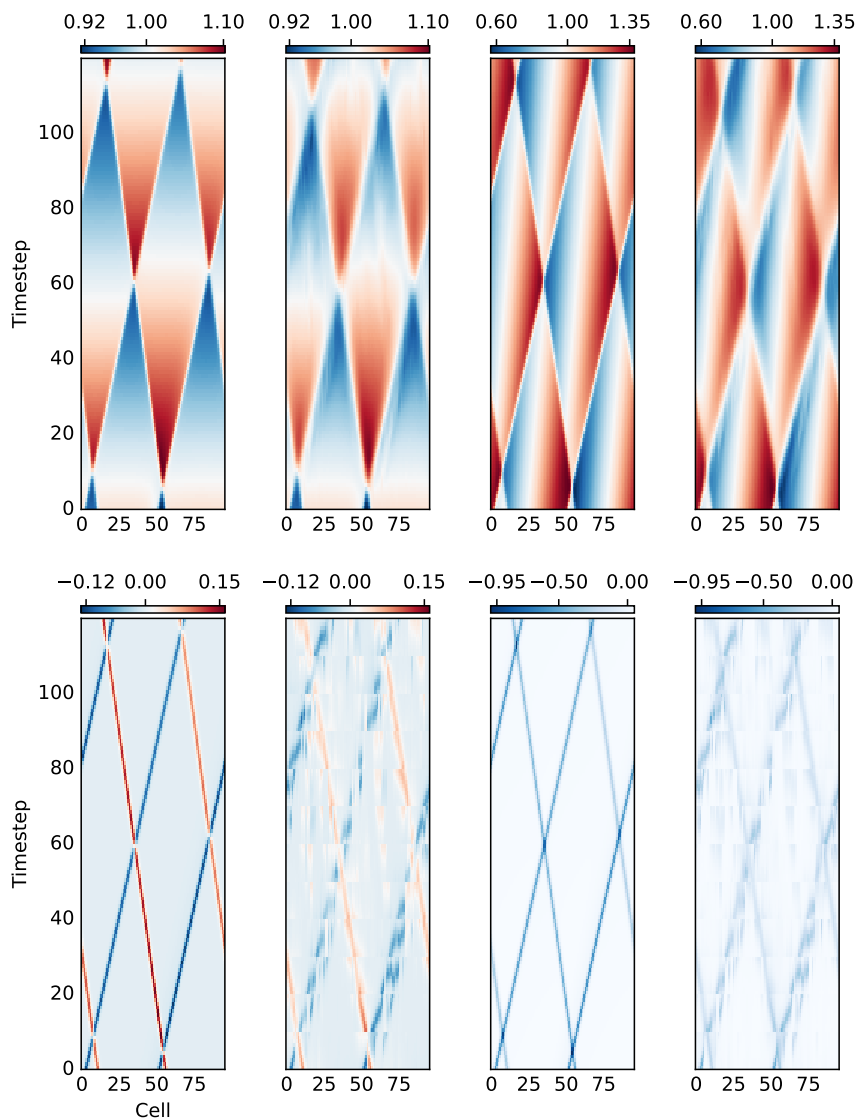


FIG. 2. Space-time heatmaps for trajectory with $\delta = 0.75$. The layout of the plots is as in Figure 1.

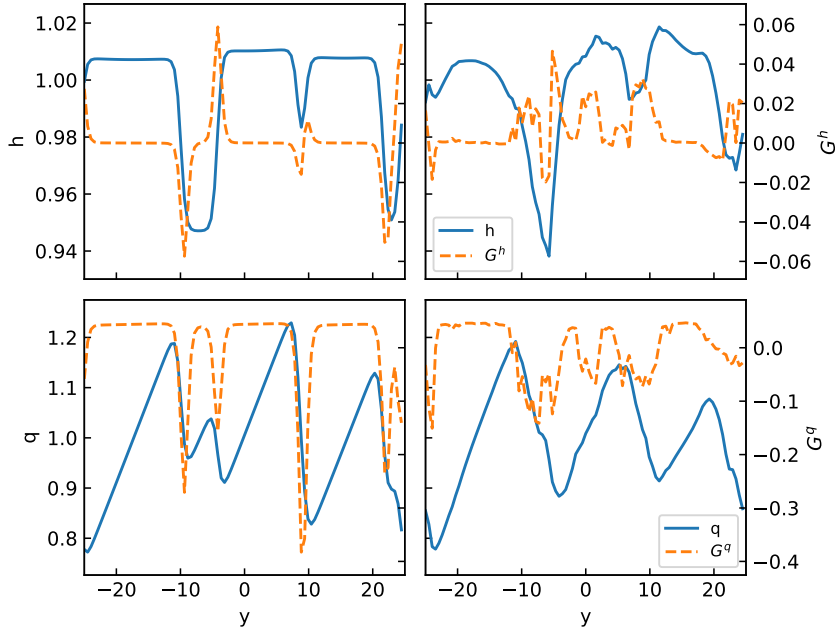


FIG. 3. Spatial profiles of final snapshot for trajectory with $\delta = 0.25$. Top row is the results for resolved state and fluxes for the height variable; bottom row for the momentum variable. In each row, true results are on the left subplot, predicted results on the right subplot. Within each subplot, full lines are used for the resolved state with their values indicated on the left axis; dashed lines are used for the corresponding fluxes with their values indicated on the right axis.

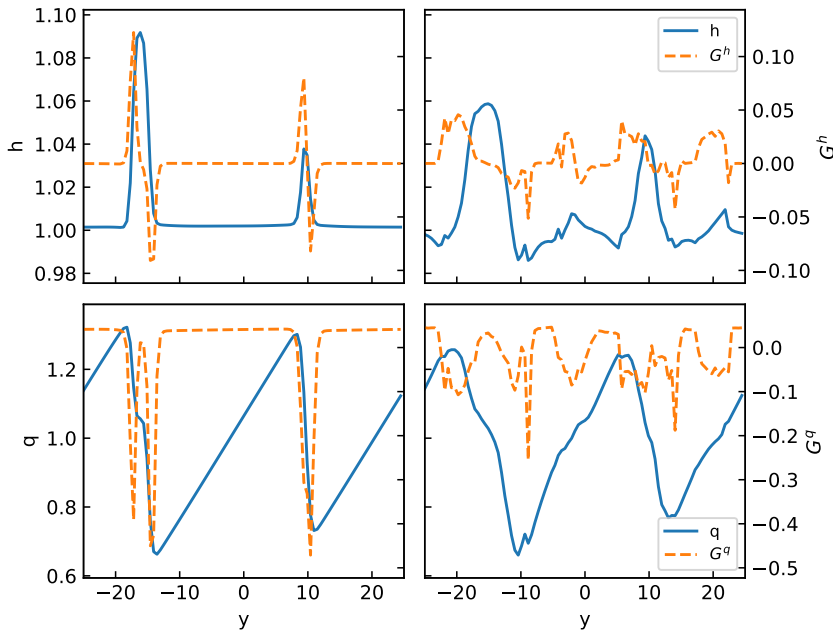


FIG. 4. Spatial profiles of final snapshot for trajectory with $\delta = 0.75$. The layout of the plots is as in Figure 3.